HAL
open science

Structural insight into the formation of lipoprotein-β-barrel complexes.

Raquel Rodríguez-Alonso, Juliette Létoquart, van Son Nguyen, Gwennaelle Louis, Antonio Calabrese, Bogdan Iorga, Sheena Radford, Seung-Hyun Cho, Han Remaut, Jean-Francois Collet

To cite this version:

Raquel Rodríguez-Alonso, Juliette Létoquart, van Son Nguyen, Gwennaelle Louis, Antonio Calabrese, et al.. Structural insight into the formation of lipoprotein-β-barrel complexes.. Nature Chemical Biology, 2020, 16, pp.1019-1025. 10.1038/s41589-020-0575-0 . hal-02879863

HAL Id: hal-02879863

https://hal.science/hal-02879863

Submitted on 10 Nov 2020

HAL is a multi-disciplinary open access archive for the deposit and dissemination of scientific research documents, whether they are published or not. The documents may come from teaching and research institutions in France or abroad, or from public or private research centers.

L'archive ouverte pluridisciplinaire **HAL**, est destinée au dépôt et à la diffusion de documents scientifiques de niveau recherche, publiés ou non, émanant des établissements d'enseignement et de recherche français ou étrangers, des laboratoires publics ou privés.

Structural insight into the formation of lipoprotein-β-barrel complexes

Raquel Rodríguez-Alonso[1,2,7], Juliette Létoquart[1,2,7], Van Son Nguyen[3,4], Gwennaelle Louis[1,2], Antonio N. Calabrese[5], Bogdan I. Iorga[6], Sheena E. Radford[5], Seung-Hyun Cho[1,2,*], Han Remaut[3,4,*] and Jean-François Collet[1,2,*]

[1]WELBIO - Walloon Excellence in Life Sciences and Biotechnology, Avenue Hippocrate 75, 1200 Brussels, Belgium

[2]de Duve Institute, Université catholique de Louvain, Avenue Hippocrate 75, 1200 Brussels, Belgium

[3]Structural Biology Brussels, Vrije Universiteit Brussel, 1050 Brussels, Belgium

[4]Structural and Molecular Microbiology, Structural Biology Research Center, VIB, 1050 Brussels, Belgium

[5]Astbury Centre for Structural Molecular Biology, School of Molecular and Cellular Biology, Faculty of Biological Sciences, University of Leeds, Leeds LS2 9JT, UK

[6]Université Paris-Saclay, CNRS UPR 2301, Institut de Chimie des Substances Naturelles, 91198 Gif-sur-Yvette, France

[7]co-first authors

*Correspondence: seung.cho@uclouvain.be, han.remaut@vub.be, and jfcollet@uclouvain.be

The β-barrel assembly machinery (BAM) inserts outer membrane β-barrel proteins (OMPs) in the outer membrane of Gram-negative bacteria. In Enterobacteriacea, BAM also mediates export of the stress sensor lipoprotein RcsF to the cell surface by assembling RcsF-OMP complexes. Here, we report the crystal structure of the key BAM component BamA in complex with RcsF. BamA adopts an inward-open

conformation, with the lateral gate to the membrane closed. RcsF is lodged deep inside the lumen of the BamA barrel, binding regions proposed to undergo an outward and lateral opening during OMP insertion. On the basis of our structural and biochemical data, we propose a push-and-pull model for RcsF export upon conformational cycling of BamA and provide a mechanistic explanation for how RcsF uses its interaction with BamA to detect envelope stress. Our data also suggest that the flux of incoming OMP substrates is involved in the control of BAM activity.

Introduction

The vast majority of proteins inserted in the outer membrane of Gram-negative bacteria adopt a β-barrel conformation. Their assembly depends on the activity of the conserved β-barrel assembly machinery (BAM), whose core component is the OMP85-family protein BamA [1,2]. BamA is an outer membrane 16-stranded β-barrel with a large periplasmic extension consisting of five POlypeptide TRansport-Associated (POTRA) domains at its N-terminus [1]. Structures of BAM have shown that BamA can adopt two conformations: an outward-open conformation [3,4], in which the β-barrel domain opens between strands β1 and β16 to form a lateral gate to the membrane, and an inward-open conformation [5,6], in which the lateral gate is sealed while a periplasmic entry pore to the barrel lumen is open. In the bacterium *Escherichia coli*, four accessory lipoproteins (BamB, BamC, BamD, and BamE) complete BAM, forming a pentameric holocomplex [7,8]. BamBCDE are anchored to the outer membrane by a lipid moiety but reside in the periplasm. BamB and BamD directly bind the POTRA domains of BamA, while BamC and BamE bind BamD [1,2]. Although all components are required for efficient assembly of *E. coli*'s diverse set of OMPs, only BamA and BamD are essential and conserved throughout Gram-negative bacteria [1,2]. Despite important

51 structural and functional insights during 15 years of intense scrutiny due to the essential
52 activity of BAM in generating and maintaining the outer membrane, crucial questions remain
53 unsolved regarding the mechanism of this molecular machine. In particular, the functional
54 importance of BamA cycling between the outward-open and inward-open conformations
55 remains unclear, as are the respective contributions of the various BAM components to OMP
56 assembly [9].
57
58 The primary function of BAM is the assembly of OMPs and, when necessary, the
59 translocation of their associated extracellular domains across the outer membrane. More
60 recently, BAM has also been implicated in export of the outer membrane lipoprotein RcsF to
61 the cell surface [10,11] via the assembly of complexes between this lipoprotein and three
62 abundant OMPs (OmpA, OmpC, and OmpF) [10,11]. Support for the involvement of BAM in
63 RcsF export comes from *in vivo* crosslinking experiments in which a complex between RcsF
64 and BamA, considered to be an intermediate in the formation of RcsF-OmpA/C/F complexes,
65 was trapped [10,11]. Further, in cells lacking BamB and BamE, RcsF accumulates on BamA and
66 causes a lethal block to BAM-mediated OMP assembly, suggesting that OMPs and surface-
67 exposed RcsF exploit at least partially overlapping assembly routes [12,13].
68
69 RcsF functions as an envelope stress sensor capable of mounting a protective response when
70 damage occurs in the peptidoglycan or in the outer membrane [14,15]. Interestingly, we
71 previously determined that sending RcsF to the surface is part of a cellular strategy that
72 enables RcsF to detect damage in the cell envelope. Under stress conditions, newly
73 synthesized RcsF molecules fail to interact with BamA [10]: they are not exported to the surface
74 and remain exposed to the periplasm, which allows them to trigger the Rcs signaling cascade
75 by reaching the downstream Rcs partner in the inner membrane [16]. Thus, surface exposure is

76 intimately linked to the function of RcsF. However, the molecular details of the BamA-RcsF
77 interaction, how BAM orchestrates the export of RcsF with OMP assembly, and what
78 prevents RcsF from interacting with BamA under stress conditions remain unknown. Here we
79 sought to address these questions by obtaining structural information about the interaction
80 between BamA and RcsF.
81
82 **Results**
83
84 **RcsF can be purified with the BAM complex**
85 In a series of exploratory experiments, we co-overexpressed RcsF with the BamAB sub-
86 complex, or with the BamABCDE holocomplex; both BamAB-RcsF and BamABCDE-RcsF
87 could be detergent-extracted from the membrane and purified via affinity chromatography
88 using a His-tag on the N-terminus of BamA (Fig. 1a). Using native gel electrophoresis, we
89 confirmed that RcsF binds BamABCDE, and not only BamAB (Fig. 1a, b, c). However,
90 whereas BamAB-RcsF was stable and could be purified to homogeneity by size-exclusion
91 chromatography, BamABCDE-RcsF was unstable (Extended Data Fig. 1a, b). Interesting to
92 note, destabilization of BamABCDE was only observed when RcsF was present (Extended
93 Data Fig. 1c).
94
95 **BamA is in the inward-open conformation in the structure**
96 The BamAB-RcsF complex was crystallized and its structure solved to 3.8 Å resolution by
97 molecular replacement using the structures of BamA and RcsF (PDB: 5D0O and 2Y1B,
98 respectively; Supplementary Table 1). While this structure contained BamA and RcsF (Fig.
99 2), BamB dissociated from the BamA-RcsF complex during crystallization and was absent.
100 The asymmetric unit contained two BamA-RcsF conformers, although for one of them, no

101 unambiguous electron density was observed for POTRA domains 1, 2, 3, and 5 (Extended
102 Data Fig. 2a, b). The β-barrel of BamA was found in an inward-open conformation closely
103 matching that reported in structures of *E. coli* BamABCDE ([6], with a root mean square
104 deviation of 0.9 Å for 383 equivalent Cα atoms in the BamA β-barrel of PDB: 5D0O) or
105 BamA truncates lacking POTRA domains 1-4 or 1-5 [17-20].
106
107 **RcsF is located inside the lumen of the BamA β-barrel**
108 In both BamA copies, RcsF was lodged deep inside the lumen of the BamA β-barrel (Fig. 2a;
109 Extended Data Fig. 2c). RcsF contacts two BamA loops protruding into the β-barrel: (1)
110 extracellular loop L6 (^{e}L6; ~77 Å^2 buried surface area, one putative H bond; note that at 3.8
111 Å resolution, amino-acid sidechain positions cannot be unambiguously determined), and (2)
112 the periplasmic loop connecting strands 7 and 8 (^{p}L4; ~140 Å^2 buried surface area, one
113 putative H bond) (Fig. 2, 3a). Although contacting RcsF, these loops retain a conformation
114 closely matching that seen in inward-open BamA structures (Fig. 3b). However, the main
115 BamA-RcsF contact occurs through the luminal wall of the BamA β-barrel, encompassing
116 ~1100 Å^2 of buried surface area and comprising up to 15 putative H-bonds (Fig. 2). This
117 RcsF-BamA β-barrel interaction can be divided into three zones. Zone 1 (Z1) consists of
118 perhaps nine H bonds formed by BamA residue 488 and residues 463, 465, and 466 in the
119 loop connecting β3 and β4 and contacting the RcsF loop connecting β1 and α1 ($L^{\beta1-\alpha1}$) (Fig.
120 2b, c, Fig. 3a, c). Zone 2 (Z2) is made of perhaps four H bonds formed by BamA residues
121 592 and 634, located above ^{p}L4 (Fig. 2c, 3a). β16, one of the components of the proposed
122 lateral gate of the BamA β-barrel, constitutes the third zone (Fig. 2b, c, 3a). The bottom of
123 RcsF protrudes out of the BamA β-barrel into the periplasm, residing in close proximity to
124 POTRA domains 3-5 (Fig. 2a, b). As a result, RcsF sterically pushes POTRA5 outward,
125 causing a 26° rotation compared to the inward-open conformation found in BamA structures

126 [5,6] (Fig. 3b). Although the lipid anchor of RcsF and the N-terminal disordered linker (residues
127 16-50) [21,22] are not apparent in this structure, the position of RcsF is compatible with the lipid
128 anchor residing in the inner leaflet of the outer membrane. Of note, the binding interface
129 between RcsF and BamA does not overlap with the binding sites of BamA for its accessory
130 lipoproteins (Extended Data Fig. 3). Consistent with this observation, the RcsF-BamA
131 interaction is compatible with the binding of BamBCDE, as determined experimentally (Fig.
132 1; Extended Data Fig. 1).
133
134 To validate the BamA-RcsF conformation revealed by the X-ray structure, we subjected the
135 complex to crosslinking and analysis via mass spectrometry using the homobifunctional
136 NHS-ester crosslinker disuccinimidyl dibutyric urea [23]. The sequence coverage of RcsF was
137 about 60% (Extended Data Fig. 4a). Note that one peptide from the N-terminal linker was
138 detected, indicating that the N-terminal disordered region was not degraded during
139 purification. Crosslinks were identified between lysine residues in RcsF (two lysines from
140 the globular domain and one located at the C-terminus of the linker) and those in POTRA4
141 and POTRA5 (Extended Data Fig. 4b; Supplementary Table 2), providing further support for
142 the architecture of BamA-RcsF determined by crystallography. To confirm that RcsF binds
143 inside the barrel of BamA, we incorporated the photoreactive lysine analog N6-((3-(3-
144 methyl-3H-diazirin-3-yl)propyl)carbamoyl)-L-lysine (DiZPK) [24] at multiple positions in the
145 BamA β-barrel domain, selecting residues (R583, R592, K598, K610, R632, R634, R661,
146 K808) whose sidechains face the lumen of the barrel (Extended Data Fig. 4b). After exposure
147 to ultraviolet light, RcsF efficiently crosslinked to BamA when DiZPK was incorporated at
148 three of the selected residues (R592, R598, K610) and to a lower extent at residue K808
149 (Extended Data Fig. 4b, c), confirming that RcsF binds deep inside the barrel. We measured
150 an equilibrium dissociation constant of 350±49 or 420±48 nM, respectively, depending on

151 whether BamA or RcsF was immobilized (Extended Data Fig. 4d, e). Finally, we deleted
152 loop 1, a short, non-essential [25] segment located between the first and second β-strands of the
153 barrel (residues 434 to 437; $BamA_{\Delta loop1}$) (Fig. 3a; Extended Data Fig. 4b). $BamA_{\Delta loop1}$ is
154 functional [5] and able to rescue the lethality of a Δ*bamA* deletion mutant, despite the fact that
155 the levels of major OMPs are slightly decreased in cells expressing $BamA_{\Delta loop1}$ (Extended
156 Data Fig. 4f). We hypothesized that deleting this loop would destabilize the BamA-RcsF
157 interaction because of the close proximity of loop 1 to the lateral gate area and to loop 6, two
158 regions of interaction between BamA and RcsF. As predicted, RcsF could be pulled down
159 with BamA but not with $BamA_{\Delta loop1}$ (Extended Data Fig. 4g). Further, the Rcs signaling
160 cascade, which is turned on when RcsF fails to interact with BamA [10], was constitutively
161 induced in Δ*bamA* cells complemented with $BamA_{\Delta loop1}$ (Extended Data Fig. 4h). In sum,
162 these results provide functional evidence for our structure of BamA-RcsF and confirm the
163 presence of RcsF inside the barrel of BamA.
164

165 **RcsF does not bind BamA when the lateral gate is open**

166 Strikingly, our structure suggests that RcsF binding is incompatible with the BamA β-barrel
167 residing in the outward-open conformation (Fig. 3a). Confirming this hypothesis, RcsF was
168 found to bind $BamA^{G433C/N805C}$, a mutant in which opening of the lateral gate is prevented by
169 a disulfide bond between β1 and β16 [26], but not to $BamA^{G393C/G584C}$, which is locked in the
170 outward-open conformation [5] (Extended Data Fig. 5a, b). However, when reduced,
171 $BamA^{G393C/G584C}$ returned to the inward-open conformation and regained the ability to bind
172 RcsF (Extended Data Fig. 5c). Importantly, given its ability to only bind the inward-open
173 conformation of BamA, the BamA-RcsF complex serves as a proxy for this state.
174 Interestingly, RcsF was recently reported to accumulate on BamA and to jam OMP assembly
175 in the absence of BamB and BamE [12,13]. Thus, in light of our structural findings, BamA

176 conformational cycling is likely impaired when BamB and BamE are absent. However,
177 binding of these accessory lipoproteins cannot be sufficient to trigger conformational changes
178 in BamA. The structure of BamABCDE has been solved not only in the outward-open
179 conformation but also in the inward-open conformation [3-6], despite the presence of all
180 accessory lipoproteins. In addition, we have shown here that RcsF could be co-purified with
181 BamABCDE (Fig. 1; Extended Data Fig. 1), implying that in this purified complex, BamA
182 was in the inward-open conformation. Thus, BamA can remain in the inward-open
183 conformation even when BamBCDE are present, strongly supporting the notion that BAM
184 conformational cycling is triggered by an external signal.
185
186 **OMP substrates trigger conformational cycling in BamA**
187 What is this trigger? Insights came from *in vivo* crosslinking experiments carried out in cells
188 in which the expression levels of the BAM components were only moderately increased (~2-
189 fold) compared with wild-type levels. Whereas RcsF can be crosslinked to BamA when the
190 BamA and BamB subunits are slightly over-expressed, the BamA-RcsF complex becomes
191 barely detectable when the moderate over-expression of all BAM components is induced
192 (Fig. 4 a, b). We explain this as follows: the BamAB subcomplex is not functional and does
193 not funnel RcsF to its OMP partners. As a result, BamA-RcsF accumulates and OmpA-RcsF
194 does not form (Fig. 4a). However, if all BAM components (BamABCDE) are moderately
195 overexpressed, BAM activity is restored, RcsF only transiently interacts with BamA, and
196 formation of OmpA-RcsF resumes (Fig. 4a; note that in these experiments, BAM is still
197 expressed at physiological levels from the chromosome—by using plasmids, we manipulate
198 the stoichiometry of the BAM components (Fig. 4b)). Therefore, whether a stable RcsF
199 complex forms with BAM depends critically on the rates of OMP synthesis and delivery to
200 BAM, as well as the ratio of active BAM complexes to the concentrations of OMP and RcsF

201 substrates. When we purified the BamABCDE-RcsF complex (Fig. 1; Extended Data Fig. 1),
202 all BAM components were highly over-expressed, which increased the ratio of active
203 complexes to incoming OMP substrates and allowed accumulation of RcsF on BAM. Thus,
204 our data support a model in which it is the flux of incoming OMP substrates that triggers
205 conformational changes in the BamA barrel and release of RcsF to its OMP partners (see
206 below; Fig. 4c). Although complexes have to date only been observed between RcsF and
207 OmpA/C/F [10,11], complexes may form between RcsF and other, less abundant OMPs,
208 depending on the unfolded OMP that is delivered to the BamABCDE-RcsF complex.
209

210 **RcsF is transferred to its partners during BamA cycling**

211 RcsF is not an integral component of BAM; it can bind BamA with high affinity, but it is
212 eventually funneled to OMPs and displayed on the cell surface [10,11]. It has been proposed that
213 RcsF crosses the outer membrane by being threaded through the lumens of OMPs [11]. In one
214 possible scenario, RcsF could be transferred from BamA to its OMP partner following
215 opening of the lateral gate and formation of a hybrid barrel (or another non-covalent complex
216 [9] between BamA and the nascent OMP), which then buds away from BamA, taking RcsF
217 with it. Available structures show that the transition from the inward-open to the outward-
218 open conformation of BamA encompasses a large outward rotation of strands 1-6 of the
219 BamA β-barrel, as well as a 20 Å inward displacement of POTRA 5 (Fig. 3a, b, c) [5,6].
220 Strikingly, BamA strands 1-6 coincide with the main RcsF-BamA interaction zone (Z1) seen
221 in our structure, such that outward rotation of Z1 may exert a pulling force on the tip of RcsF
222 (Fig. 3a, c). Concomitantly, the inward movement of POTRA5 would exert a pushing force
223 on the bottom of RcsF (Fig. 3c). We therefore hypothesize that during the inward-to-outward
224 transition of BamA, this push-and-pull action on RcsF could play a role in the transfer of
225 RcsF to its OMP partners and its translocation to the cell surface (Fig. 4c). Supporting this,

226 dynamic importance sampling simulations in which BamA transitions from the inward-open
227 conformation (as in our structure) to the outward-open conformation (PDB code 5D0Q) show
228 POTRA5 moving towards the periplasmic exit of the lumen, pushing RcsF upwards. The
229 movement of POTRA5 is accompanied later on by the movement of Z1, opening the
230 outward-facing extremity (Extended Data Fig. 6a, b, c, d and Supplementary Video).
231 Furthermore, by introducing a short peptide in the hinge between POTRA5 and the β-barrel
232 domain of BamA ($BamA^{hinge}$), we could confirm the functional importance of this region for
233 BamA activity. We found indeed that expression of $BamA^{hinge}$ from a plasmid rescues the
234 growth of Δ*bamA* cells in minimal media at 30°C but not in rich media at 37°C, indicating
235 that $BamA^{hinge}$ is unable to cope with the rate of OMPs folding in these latter conditions
236 (Extended Data Fig. 6e).
237
238 **Discussion**
239
240 Our work reveals how BamA interacts with RcsF, providing insights into the mechanism
241 used by BAM to assemble RcsF-OMP complexes, a novel activity by which BAM exports
242 this lipoprotein to the cell surface. It would be surprising if an essential machinery such as
243 BAM—with a global role in formation of the cell envelope—was only dedicated to export
244 RcsF to the surface. Hence, it is tempting to speculate that other lipoproteins may follow the
245 same route and decorate the surface of *E. coli,* in contrast to the general view that outer
246 membrane lipoproteins face the periplasm [27].
247
248 By showing that the globular domain of RcsF is lodged deep inside the barrel of BamA, our
249 structure also reveals the remarkable—and unanticipated —finding that the BamA β-barrel
250 can accommodate a lipoprotein "substrate" with a globular domain 12 kDa in size. This

finding further establishes BAM as an essential hub that contributes to outer membrane biogenesis by interacting both with nascent OMPs for assembly and lipoproteins for export. Future work will reveal whether other lipoproteins bind BamA in a way similar to RcsF and also clarify the topology of the RcsF-OMP complexes. It has indeed been proposed that the lipid moiety of RcsF is anchored in the outer leaflet of the membrane and that the N-terminal disordered linker is exposed on the cell surface before being threaded through the lumens of the OMPs [11]. In this model, the globular domain of RscF resides inside the periplasm. Although we cannot rule out that RcsF flips during release from BamA and transfer to its OMP partners, our structure is more consistent with the hypothesis that BamA releases the globular domain of RcsF on the cell surface. Further investigation will therefore be needed to answer this question, and whether the location of RcsF depends on the identity of its OMP partner.

It is also remarkable that RcsF binds the lateral gate area and the outward rotating region of the BamA barrel, sites that sense BAM conformational cycling triggered by incoming OMP substrates. We previously reported that RcsF uses its interaction with BamA to detect stress in the cell envelope: when damage occurs in the peptidoglycan or the outer membrane, newly synthesized RcsF molecules fail to interact with BamA, activating the Rcs stress response [10]. Our structure provides a possible explanation for this scenario by suggesting that BamA preferentially adopts the outward-open conformation when envelope integrity is impaired, which would *de facto* prevent RcsF binding and promote Rcs activation. Thus, we propose that cells could monitor envelope integrity via the conformational cycling of BamA.

How the outer membrane of Gram-negative bacteria is assembled remains a long-standing mystery and a crucial question in biology. Here, we focused on BamA, the core component

276 of BAM whose activity is essential to constructing and maintaining the outer membrane. By
277 solving the structure of BamA in complex with its lipoprotein substrate RcsF, our work sheds
278 new light on BAM. It not only provides crucial molecular insights into how BAM exports
279 lipoproteins to the surface, but also uncovers important new features of this essential
280 machinery and its mechanism. Because BAM activity is required for bacterial survival, the
281 complex is an attractive target for new antibiotics [28-31]. Our work also paves the way to the
282 design of new antibacterials that interfere with BAM conformational cycling, because
283 blocking BAM in the inward-open conformation lethally jams BAM with RcsF.
284

285 **ACKNOWLEDGMENTS**

286 We thank Asma Boujtat for technical help. We are indebted to Dr. Peng R. Chen (Peking
287 University) for sharing DiZPK, to Dr. Harris Bernstein (NIH, Bethesda, USA) for providing
288 strains and plasmids, and to Dr. Michael Deghelt, Dr. Géraldine Laloux, Dr. Camille
289 Goemans (EMBL, Heidelberg, Germany), and Dr. Pauline Leverrier for helpful suggestions
290 and discussions and for providing comments on the manuscript. We thank Pierre Legrand and
291 staff at Soleil Synchrotron France and at Diamond Light Source UK for beamtime and their
292 assistance during data collection. This work was supported, in part, by grants from the Fonds
293 de la Recherche Scientifique – FNRS, from the FRFS-WELBIO grants n° WELBIO-CR-
294 2015A-03 and WELBIO-CR-2019C-03, from the EOS Excellence in Research Program of
295 the FWO and FRS-FNRS (G0G0818N), from the Fédération Wallonie-Bruxelles (ARC
296 17/22-087), from the European Commission via the International Training Network
297 Train2Target (721484), from the French region Ile-de-France (DIM Malinf) and from the
298 BBSRC (BB/P000037/1, BB/M012573/1).
299

300 **AUTHOR CONTRIBUTIONS**

J.-F.C., R.R.A., S.E.R., H.R., and S.H.C. wrote the manuscript. J.L., RRA, S.N., G.L., S.H.C., H.R., and J.-F.C. designed the experiments. J.L., R.R.A., S.N., G.L., and S.H.C. performed the experiments, constructed the strains, and cloned the constructs. B.I. performed the dynamic importance sampling simulations. J.L., R.R.A., S.N., S.H.C., H.R., and J.-F.C. analyzed and interpreted the data. A.N.C. and S.E.R. performed and analyzed the crosslinking mass spectrometry experiments. All authors discussed the results and commented on the manuscript.

AUTHOR INFORMATION

The authors declare no competing financial interests.

DATA AVAILABILITY

Coordinates and structure factors have been deposited in the Protein Data Bank under accession number 6T1W. All other data generated or analysed during this study are included in this published article and its supplementary information file.

REFERENCES

1 Noinaj, N., Gumbart, J. C. & Buchanan, S. K. The beta-barrel assembly machinery in motion. *Nat Rev Microbiol* **15**, 197-204, doi:10.1038/nrmicro.2016.191 (2017).

2 Hagan, C. L., Silhavy, T. J. & Kahne, D. beta-Barrel membrane protein assembly by the Bam complex. *Annu Rev Biochem* **80**, 189-210, doi:10.1146/annurev-biochem-061408-144611 (2011).

3 Iadanza, M. G. *et al.* Lateral opening in the intact beta-barrel assembly machinery captured by cryo-EM. *Nat Commun* **7**, 12865, doi:10.1038/ncomms12865 (2016).

4 Bakelar, J., Buchanan, S. K. & Noinaj, N. The structure of the beta-barrel assembly machinery complex. *Science* **351**, 180-186, doi:10.1126/science.aad3460 (2016).

5 Gu, Y. *et al.* Structural basis of outer membrane protein insertion by the BAM complex. *Nature* **531**, 64-69, doi:10.1038/nature17199 (2016).

6 Han, L. *et al.* Structure of the BAM complex and its implications for biogenesis of outer-membrane proteins. *Nat Struct Mol Biol* **23**, 192-196, doi:10.1038/nsmb.3181 (2016).

7 Wu, T. *et al.* Identification of a multicomponent complex required for outer membrane biogenesis in Escherichia coli. *Cell* **121**, 235-245 (2005).

8 Sklar, J. G. *et al.* Lipoprotein SmpA is a component of the YaeT complex that assembles outer membrane proteins in Escherichia coli. *Proc Natl Acad Sci U S A* **104**, 6400-6405 (2007).

9 Schiffrin, B., Brockwell, D. J. & Radford, S. E. Outer membrane protein folding from an energy landscape perspective. *BMC Biol* **15**, 123, doi:10.1186/s12915-017-0464-5 (2017).

10 Cho, S. H. *et al.* Detecting Envelope Stress by Monitoring beta-Barrel Assembly. *Cell* **159**, 1652-1664, doi:10.1016/j.cell.2014.11.045 (2014).

11 Konovalova, A., Perlman, D. H., Cowles, C. E. & Silhavy, T. J. Transmembrane domain of surface-exposed outer membrane lipoprotein RcsF is threaded through the lumen of beta-barrel proteins. *Proc Natl Acad Sci U S A* **111**, E4350-4358, doi:10.1073/pnas.1417138111 (2014).

12 Tata, M. & Konovalova, A. Improper Coordination of BamA and BamD Results in Bam Complex Jamming by a Lipoprotein Substrate. *MBio* **10**, doi:10.1128/mBio.00660-19 (2019).

13 Hart, E. M., Gupta, M., Wuhr, M. & Silhavy, T. J. The Synthetic Phenotype of DeltabamB DeltabamE Double Mutants Results from a Lethal Jamming of the Bam Complex by the Lipoprotein RcsF. *MBio* **10**, doi:10.1128/mBio.00662-19 (2019).

14 Wall, E., Majdalani, N. & Gottesman, S. The Complex Rcs Regulatory Cascade. *Annu Rev Microbiol* **72**, 111-139, doi:10.1146/annurev-micro-090817-062640 (2018).

15 Laloux, G. & Collet, J. F. "Major Tom to ground control: how lipoproteins communicate extra-cytoplasmic stress to the decision center of the cell". *J Bacteriol*, doi:10.1128/JB.00216-17 (2017).

16 Hussein, N. A., Cho, S. H., Laloux, G., Siam, R. & Collet, J. F. Distinct domains of Escherichia coli IgaA connect envelope stress sensing and down-regulation of the Rcs phosphorelay across subcellular compartments. *PLoS Genet* **14**, e1007398, doi:10.1371/journal.pgen.1007398 (2018).

17 Kaur, H. *et al.* Identification of conformation-selective nanobodies against the membrane protein insertase BamA by an integrated structural biology approach. *J Biomol NMR* **73**, 375-384, doi:10.1007/s10858-019-00250-8 (2019).

18 Albrecht, R. *et al.* Structure of BamA, an essential factor in outer membrane protein biogenesis. *Acta Crystallogr D Biol Crystallogr* **70**, 1779-1789, doi:10.1107/S1399004714007482 (2014).

19 Ni, D. *et al.* Structural and functional analysis of the beta-barrel domain of BamA from Escherichia coli. *FASEB J* **28**, 2677-2685, doi:10.1096/fj.13-248450 (2014).

20 Hartmann, J. B., Zahn, M., Burmann, I. M., Bibow, S. & Hiller, S. Sequence-Specific Solution NMR Assignments of the beta-Barrel Insertase BamA to Monitor Its Conformational Ensemble at the Atomic Level. *J Am Chem Soc* **140**, 11252-11260, doi:10.1021/jacs.8b03220 (2018).

21 Leverrier, P. *et al.* Crystal structure of the outer membrane protein RcsF, a new substrate for the periplasmic protein-disulfide isomerase DsbC. *J Biol Chem* **286**, 16734-16742, doi:10.1074/jbc.M111.224865 (2011).

22 Rogov, V. V., Rogova, N. Y., Bernhard, F., Lohr, F. & Dotsch, V. A disulfide bridge network within the soluble periplasmic domain determines structure and function of the outer membrane protein RCSF. *J Biol Chem* **286**, 18775-18783, doi:10.1074/jbc.M111.230185 (2011).

23 Calabrese, A. N. & Radford, S. E. Mass spectrometry-enabled structural biology of membrane proteins. *Methods* **147**, 187-205, doi:10.1016/j.ymeth.2018.02.020 (2018).

24 Zhang, M. *et al.* A genetically incorporated crosslinker reveals chaperone cooperation in acid resistance. *Nat Chem Biol* **7**, 671-677, doi:10.1038/nchembio.644 (2011).

25 Gu, Y., Zeng, Y., Wang, Z. & Dong, C. BamA beta16C strand and periplasmic turns are critical for outer membrane protein insertion and assembly. *Biochem J* **474**, 3951-3961, doi:10.1042/BCJ20170636 (2017).

26 Noinaj, N., Kuszak, A. J., Balusek, C., Gumbart, J. C. & Buchanan, S. K. Lateral opening and exit pore formation are required for BamA function. *Structure* **22**, 1055-1062, doi:10.1016/j.str.2014.05.008 (2014).

27 Okuda, S. & Tokuda, H. Lipoprotein sorting in bacteria. *Annu Rev Microbiol* **65**, 239-259, doi:10.1146/annurev-micro-090110-102859 (2011).

28 Storek, K. M. *et al.* Monoclonal antibody targeting the beta-barrel assembly machine of Escherichia coli is bactericidal. *Proc Natl Acad Sci U S A* **115**, 3692-3697, doi:10.1073/pnas.1800043115 (2018).

29 Imai, Y. *et al.* A new antibiotic selectively kills Gram-negative pathogens. *Nature* **576**, 459-464, doi:10.1038/s41586-019-1791-1 (2019).

30 Luther, A. *et al.* Chimeric peptidomimetic antibiotics against Gram-negative bacteria. *Nature* **576**, 452-458, doi:10.1038/s41586-019-1665-6 (2019).

31 Hart, E. M. *et al.* A small-molecule inhibitor of BamA impervious to efflux and the outer membrane permeability barrier. *Proc Natl Acad Sci U S A* **116**, 21748-21757, doi:10.1073/pnas.1912345116 (2019).

32 Majdalani, N., Hernandez, D. & Gottesman, S. Regulation and mode of action of the second small RNA activator of RpoS translation, RprA. *Mol Microbiol* **46**, 813-826 (2002).

33 Baba, T. *et al.* Construction of Escherichia coli K-12 in-frame, single-gene knockout mutants: the Keio collection. *Mol Syst Biol* **2**, 2006 0008, doi:msb4100050 [pii] 10.1038/msb4100050 (2006).

422

423

424

425

426

427

428

429

430 **LEGENDS TO THE FIGURES**

431

432 **Figure 1. RcsF forms a complex with BamAB and BamABCDE. (a, b)** SDS-PAGE (a)
433 and blue native (b) analysis of purified BAM, BAM-RcsF and BamAB-RcsF complexes
434 obtained via BamA-affinity chromatography. The bands analyzed in (c) are labelled 1 to 8.
435 **(c)** SDS-PAGE analysis of the complexes shown in panel b (bands 1 to 8). The BAM
436 complex expressed from pRRA1 is a mixture of BamABCDE and BamABDE. n= 4
437 biologically independent experiments.

438

439 **Figure 2. Structure of the BamA-RcsF complex. (a)** Ribbon diagram of the BamA-RcsF
440 complex in side view. BamA, gold; RcsF, blue. **(b, c)** Front (b) and extracellular (c) views of
441 BamA-RcsF, with RcsF shown as a solvent-accessible surface. POTRA domains 1 and 2
442 have been omitted for clarity. BamA ^{e}L6, green; ^{p}L4, magenta. Putative RcsF-interacting
443 residues in contact zones Z1 and Z2 of the BamA β-barrel are colored cyan and magenta,
444 respectively, and shown as sticks. Strands β1 and β16, which form the proposed "lateral
445 gate" of the BamA β-barrel [1], are yellow. **(d)** Periplasmic view of the BamA-RcsF complex,

446 with the BamA β-barrel shown as a solvent-accessible surface and RcsF as a ribbon. Colors
447 are as in panels b and c. POTRA domains were omitted for clarity.
448
449 **Figure 3. Conformational characteristics of the BamA-RcsF complex. (a, c)** Tilted top
450 view and slabbed side view of the overlay of the BamA-RcsF complex and BamA in the
451 outward-open conformation (grey, taken from BamACDE complex PDB:5EKQ [4]). The
452 BamA β-barrel undergoes a ~45° outward rotation at strands β1-β6, and a 20 Å inward
453 displacement of POTRA5 compared to the structure of BamA-RcsF presented here. **(b)**
454 Slabbed side view of the overlay of BamA-RcsF and BamA in the inward-open conformation
455 (grey, taken from BamABCDE complex PDB:5D0O [5]). In the structure of BamA-RcsF
456 presented here, POTRA5 makes a 26° outward rotation relative to R421, where it connects to
457 the BamA β-barrel. **(a-c)** Color scheme for BamA-RcsF is as in Fig. 2b. RcsF is shown as a
458 solvent-accessible surface (a) or a ribbon (b, c). Panels (b, c) show side views, slabbed down
459 to view the interior of the complex. For 5EKQ and 5D0O, the BAM accessory proteins
460 BamB, C, D, and E were omitted for clarity, as were POTRA domains 1-4 in all shown
461 BamA structures.
462
463 **Figure 4. BamA-RcsF is a proxy for the inward-open conformation of BamA. (a)** *In vivo*
464 chemical crosslinking of RcsF with BamA and OmpA. The BamA-RcsF complex
465 accumulates when either BamA alone or BamAB together are moderately over-expressed
466 from a plasmid in cells also expressing BAM at physiological levels from the chromosome.
467 The copies of BamA and BamAB in excess are not functional (BamCDE is required for
468 BAM activity) and do not funnel RcsF to its OMP partners. As a result, RcsF accumulates on
469 BamA and OmpA-RcsF does not form. Over-expression of BamCDE (also from a plasmid)
470 in these cells restores the stoichiometry between the BAM components: BamA-RcsF does not

471 accumulate and the formation of OmpA-RcsF is restored. As shown previously [10], levels of
472 OmpA-RcsF are inversely correlated with BamA-RcsF. Overexpression of the BamCDE sub-
473 complex alone does not impact the activity of the BAM complex expressed from the
474 chromosome: wild-type BamA-RcsF and OmpA-RcsF levels are observed. Wild-type BamA-
475 RcsF and OmpA-RcsF levels are also detected when BamA and BamCDE are overexpressed
476 together, as expected given that BamB is not essential. RcsF also forms a complex with the
477 abundant lipoprotein Lpp (Lpp-RcsF), as in [10]. Protein expression levels of OmpA were
478 analyzed by immunoblot in the non-crosslinked samples, showing no differences. The
479 additional bands that are detected in the lanes where BamA-RcsF is not observed likely
480 correspond to poorly abundant complexes between RcsF and unknown proteins. n= 3
481 biologically independent experiments. **(b)** Protein expression levels of BamB, BamC, BamD,
482 BamE and RcsF from no-crosslinked samples overexpressing BamA (pBamA), BamAB
483 (pBamA-B) and BamCDE (pSC263) were analyzed by western blot. EF-Tu expression levels
484 were analyzed as loading control. n= 3 biologically independent experiments. (**c**) Model
485 proposing that BamA conformational cycling is triggered by incoming OMP substrates on the
486 BAM holocomplex. A BamA inward-to-outward open transition could result in an upward
487 displacement of RcsF via a push-and-pull mechanism, resulting in an OMP-RcsF complex.
488 The push-and-pull mechanism involves BamA POTRA5 (P5) and Z1. The topology of the
489 OMP-RcsF complex remains to be established. For clarity, POTRA1-4 and the BAM
490 lipoproteins have been ommitted.

491

Figure 1

492

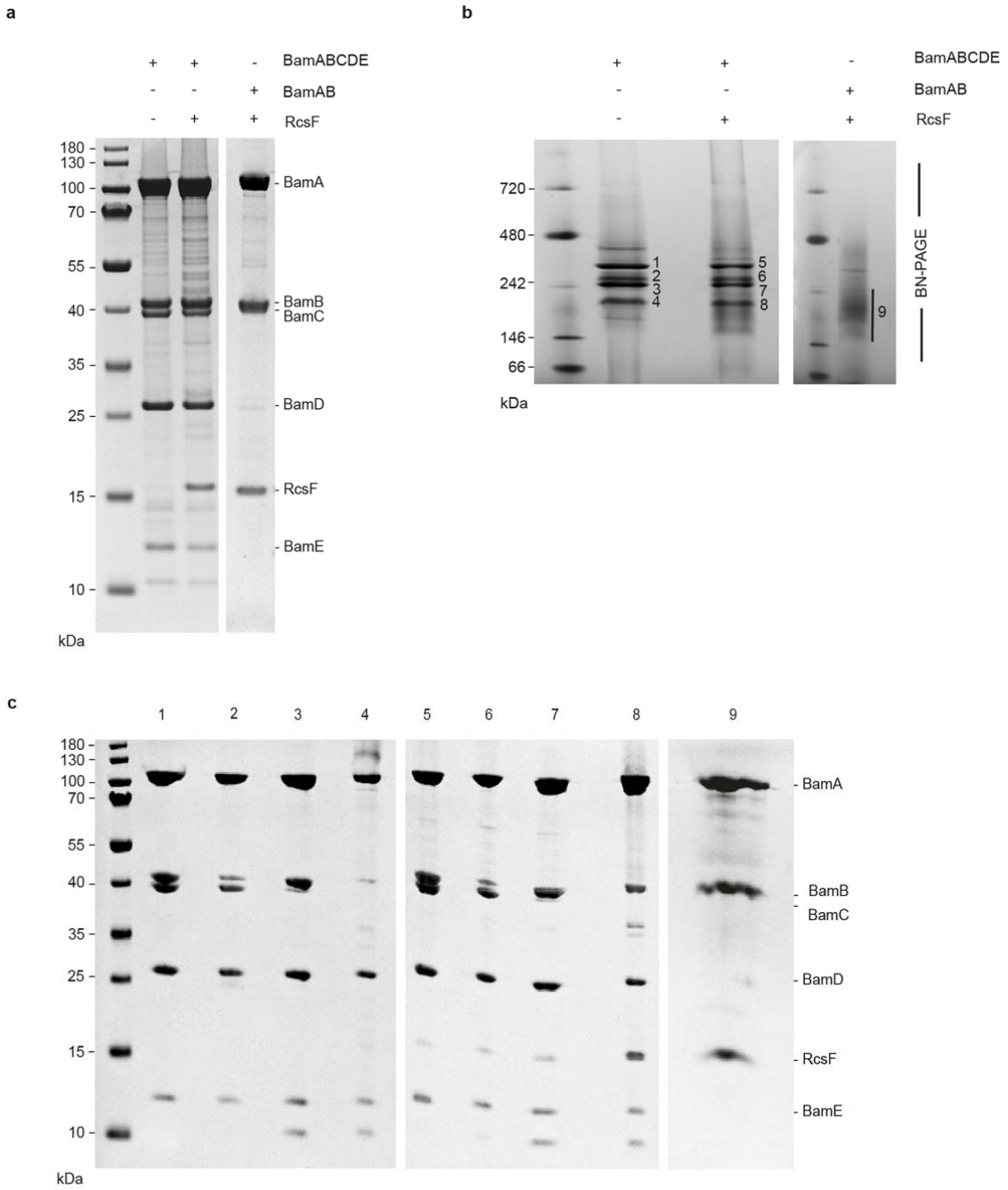

Figure 2

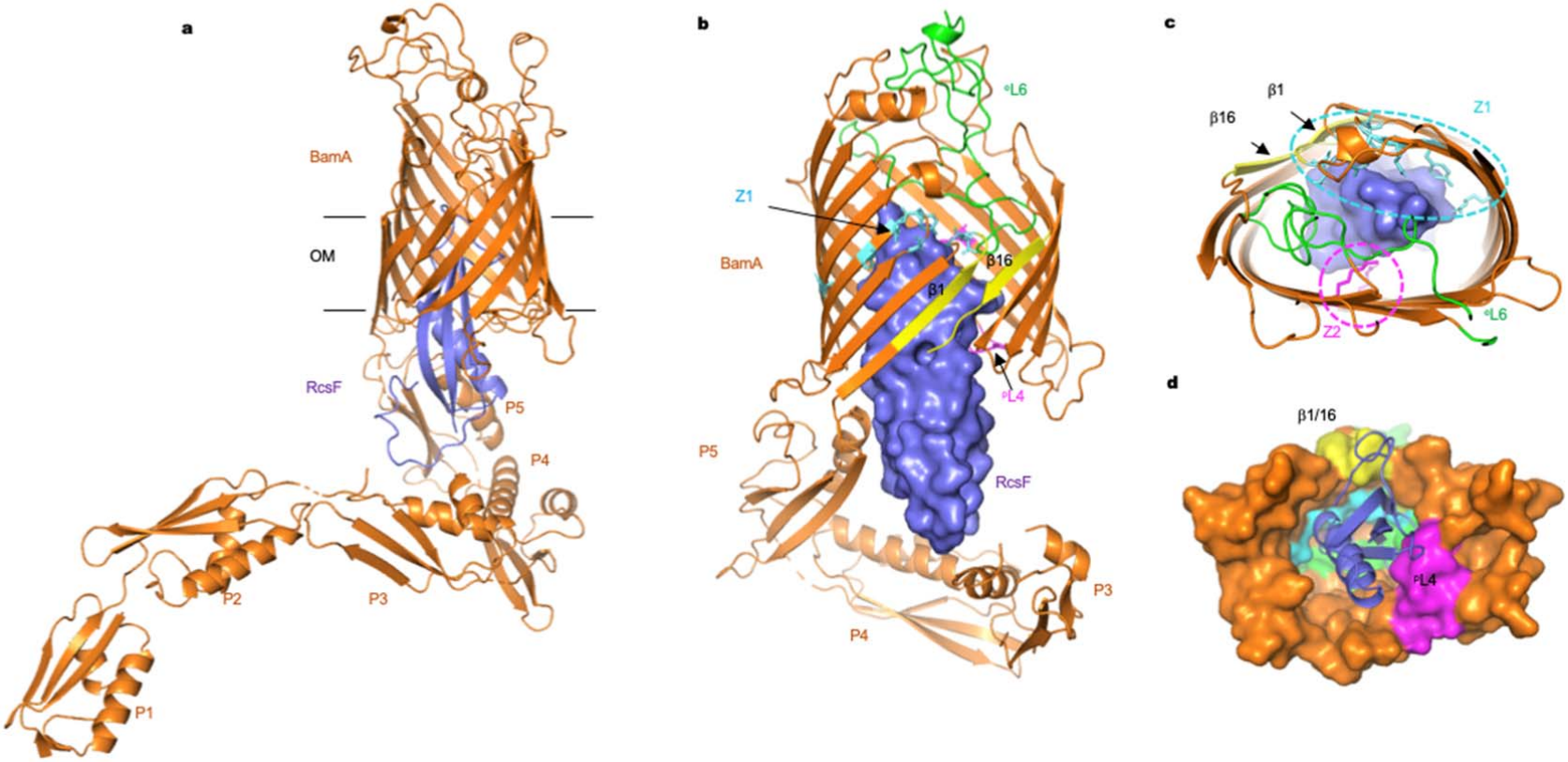
a
BamA
OM
RcsF
P5
P4
P2
P3
P1
b
ᵉL6
Z1
BamA
β16
β1
ᵉL4
P5
RcsF
P3
P4
c
β1
β16
Z1
Z2
ᵉL6
d
β1/16
ᵉL4

Figure 3

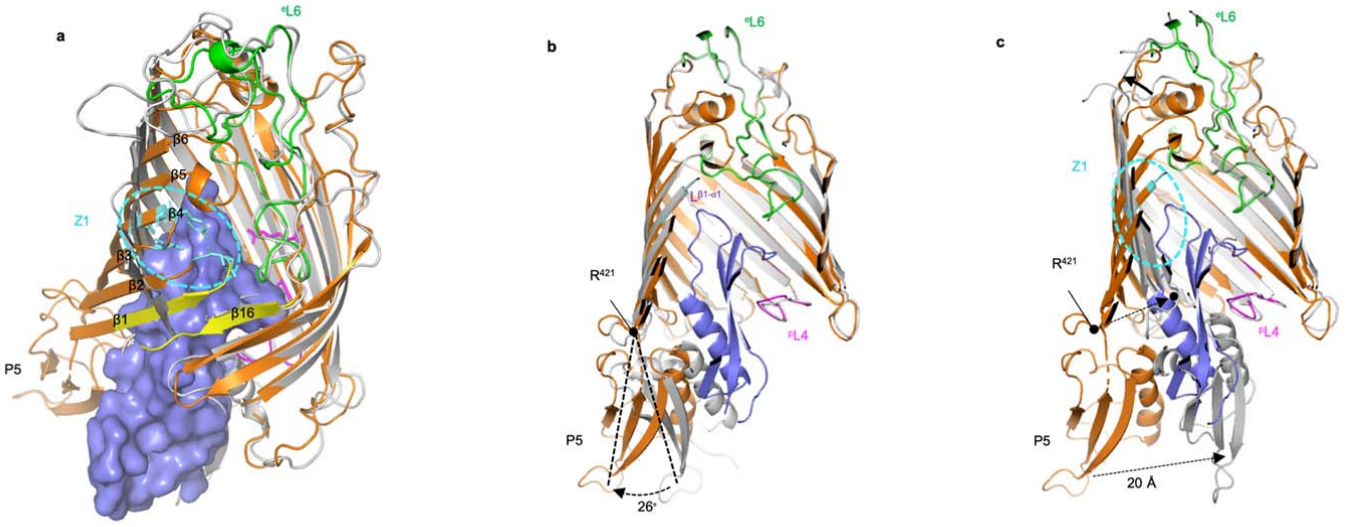
a
ºL6
β6
β5
β4
Z1
β3
β2
β1
β16
P5
b
ºL6
Lβ1-α1
R421
ºL4
P5
26°
c
ºL6
Z1
R421
ºL4
P5
20 Å

Figure 4

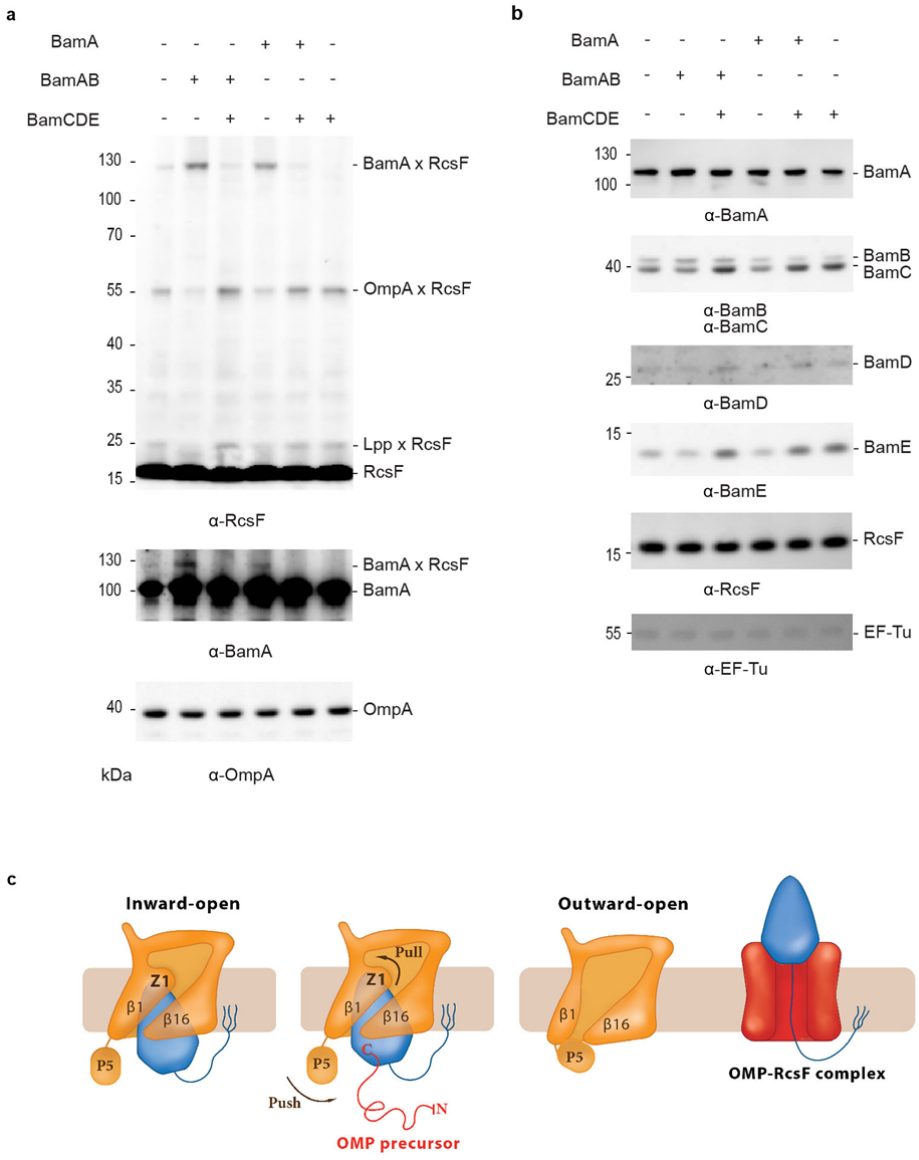
a
BamA
BamAB
BamCDE
130
100
70
55
40
35
25
15
BamA x RcsF
OmpA x RcsF
Lpp x RcsF
RcsF
α-RcsF
BamA x RcsF
BamA
α-BamA
OmpA
kDa
α-OmpA
b
BamA
BamAB
BamCDE
130
100
BamA
α-BamA
40
BamB
BamC
α-BamB
α-BamC
25
BamD
α-BamD
15
BamE
α-BamE
15
RcsF
α-RcsF
55
EF-Tu
α-EF-Tu
c
Inward-open
Z1
β1
β16
P5
Pull
Push
C
N
OMP precursor
Outward-open
OMP-RcsF complex

METHODS

Bacterial strains, plasmids, and primers

Bacterial strains and plasmids used in this study are listed in Supplementary Tables 3 and 4, respectively. The parental *E. coli* strain DH300 is a MG1655 derivative deleted for the *lac* region and carrying a chromosomal *rprA*$_P$::*lacZ* fusion at the λ phage attachment site to monitor Rcs activation [32]. To delete *bamA* on the chromosome, a kanamycin resistance (*kan*) cassette [33] with the flanking regions of *bamA* was PCR amplified from the genomic DNA of a *ΔrcsF::kan* strain (PL339) using primers "bamA Km del F" and "bamA Km del R". Then we performed λ-Red recombineering [34] with plasmid pSIM5-tet [35] on the strain containing pSC270 as a *bamA*-complementing plasmid in DH300. Deletion of *bamA* was verified by PCR. After preparing P1 lysate from this strain, *bamA* deletion (by transferring the *kan* cassette) was performed via P1 phage transduction of the appropriate strains.

We performed site-directed mutagenesis to generate *bamA* variants on plasmids. For single-codon changes, primer sequences are available upon request; otherwise see Supplementary Table 5. By using pJH114 as a template and performing site-directed mutagenesis (SDM), we introduced a six-histidine tag at the N-terminus of BamA. The C-terminal His-tag of BamE was also removed via SDM, generating pRRA1. The primer pairs were "SDM-HisBamA F" with "SDM-HisBamA R" and "bamE delHis F" with "bamE delHis R". To add *bamB* next to *bamA* in pBamA, both *bamA* and *bamB* were PCR amplified as a single DNA fragment from pJH114 [36] using primers "pTrc-for" and "bamB (NotI) R". The PCR product and pBamA were digested with NcoI and NotI and then ligated, yielding pBamA-B. pBamA^{hinge} plasmid was generated by SDM

518 using primers “BamA hinge F” and “BamA hinge R” and pBamA as template. To
519 clone *bamC*, *bamD*, and *bamE* as an operon into a low-copy plasmid (pAM238), PCR
520 was performed on pRRA1 as a template using primers “bamC kpnI F” and “pTrc-rev2”.
521 The PCR product and pAM238 were digested with KpnI and XbaI and ligated,
522 generating pSC263. We cloned *bamA* without the six-histidine tag into the low-copy
523 plasmid pSC23 [10], yielding pSC270. *bamA* was PCR amplified from *E. coli* genomic
524 DNA using primers “BamA (PciI)F” and “BamA (XbaI)R” and ligated with pSC231
525 predigested with NcoI and XbaI. To generate the *bamA* variants locked in the closed
526 and open conformations, SDM was performed on pBamA-B. First, the two cysteines in
527 the ^{e}L6 loop of BamA were mutated to serines, generating pBamA$_{L6}$-B. This plasmid
528 was used as template for SDM to generate pBamA$^{G393C/G584C}$-B and pBamA$^{G433C/N805C}$-
529 B. To generate *bamA* variants with amber codons (TAG) to insert 3-(3-methyl-3H-
530 diazirine-3-yl)-propaminocarbonyl-Nε-L-lysine (DiZPK; Artis Chemistry, Shanghai) at
531 selected positions, we performed SDM on pBamA-B and pSC270; primer sequences are
532 available upon request.
533
534 **Expression and purification of the BamAB-RcsF complex**
535 *E. coli* PL358 cells harboring pJH118 expressing N-terminal six-histidine-tagged BamA
536 and BamB [36] and pSC216 expressing RcsF [10] were cultured to overexpress BamA,
537 BamB, and RcsF. Cells were grown in Terrific Broth Auto Inducing Medium
538 (Formedium) supplemented with 0.2% (w/v) L-arabinose at 37 °C (to induce RcsF),
539 ampicillin (200 μg/mL), and chloramphenicol (25 μg/mL). Cells (1 L) were pelleted
540 when they reached OD_{600} ~ 4, re-suspended in cold phosphate-buffered saline (25 mL)
541 containing a protease-inhibitor cocktail (Complete, Roche), and lysed by two passages
542 through a French pressure cell at 1,500 psi. The cell lysate was centrifuged for 40 min at

543 40,000 × *g* and 4 °C. After centrifugation, inner-membrane proteins were solubilized
544 using 0.5% (w/v) N-lauryl sarcosine (Sigma) in a buffer containing 20 mM Tris-HCl
545 [pH 7.5] and 150 mM NaCl for 1.5 h at 4 °C on a roller. The suspension was
546 centrifuged for 40 min at 40,000 x *g* and 4 °C, after which the inner membrane fraction
547 was in the supernatant while the outer membrane fraction remained in the pellet. Outer-
548 membrane proteins were solubilized using 1% (w/v) *n*-dodecyl-β-d-maltopyranoside
549 (DDM; Anatrace) in a buffer containing 20 mM Tris-HCl [pH 7.5], 300 mM NaCl, and
550 20 mM imidazole overnight at 4 °C on a roller. After centrifugation (40,000 x *g*, 4 °C,
551 40 min), the supernatant was mixed with Ni-NTA agarose beads (2 mL; IBA
552 Lifescience) equilibrated with 20 mM Tris-HCl [pH 7.5], 300 mM NaCl, 20 mM
553 imidazole, and 1% (w/v) DDM. After washing the resin with 10 column volumes of
554 buffer (20 mM Tris-HCl [pH 7.5], 150 mM NaCl, 20 mM imidazole, 0.6% (w/v)
555 tetraethylene glycol monooctyl ether (C8E4; Anatrace), and 0.01% (w/v) DDM),
556 proteins were eluted with 5 column volumes of the same buffer supplemented with 200
557 mM imidazole. The eluted complex was then concentrated to 1 mL using a Vivaspin 4
558 Turbo concentrator (Cut-off 5 kDa; Sartorius). A final purification step was performed
559 using size-exclusion chromatography by loading the proteins on a HiLoad 10/300
560 Superdex 200 column (GE Healthcare) using 20 mM Tris-HCl [pH 7.5], 150 mM NaCl,
561 0.6% (w/v) C8E4, and 0.01% (w/v) DDM. Peak fractions were pooled and concentrated
562 to ~30 mg/mL for crystallization.
563
564 For co-crystallization with NaI, NaI replaced NaCl in the gel-filtration buffer. Peak
565 fractions were pooled and concentrated to ~30 mg/mL using a Vivaspin 4 Turbo
566 concentrator (Sartorius).
567

568 The Blue native electrophoresis analysis of the concentrated complex was carried out on
569 a 3-12% Bis-Tris gel (Life Technologies) following the manufacturer's instructions.
570 The protein complex bands separated in the native electrophoresis were identified via
571 SDS-PAGE. Briefly, bands of interest were excised, boiled in SDS-PAGE sample
572 buffer, and applied to the top of a polyacrylamide gel.
573
574 **Expression and purification of BAM (BamABCDE) in complex with RcsF**
575 *E. coli* BL21 (DE3) was transformed with pRRA1 expressing all five BAM proteins (N-
576 terminal six-histidine-tagged BamA, BamB, BamC, BamD, and BamE) and pSC216
577 expressing RcsF for BAM and RcsF overexpression. In control cells, only pRRA1 was
578 transformed. Protein expression and purification were performed as described above
579 except that the detergent was exchanged to 0.1% (w/v) DDM during Ni-NTA affinity
580 chromatography and size-exclusion chromatography. Eluted complexes were identified
581 via SDS-PAGE and concentrated to 4 mg/mL. Blue native electrophoresis of the
582 concentrated complexes was carried out as described above.
583
584 **Crystallization, data collection and structure determination**
585 Crystallization assays were carried out using the hanging drop vapor diffusion method
586 in 48-well plates (Molecular Dimensions) at 20°C. The protein solution was mixed in a
587 2:1 ratio with the crystallization solution from the reservoir. The best native crystals
588 were grown after 4 to 5 days in C10 and G10 conditions from Morpheus crystallization
589 screen (Molecular dimensions; C10: 0.03 M sodium nitrate, 0.03 M sodium phosphate
590 dibasic, 0.03 M ammonium sulfate, 0.10 M Tris-base [pH 8.5]; BICINE, 20 % (v/v)
591 ethylene glycol; 10 % w/v PEG 8000; G10: 0.02 M sodium formate; 0.02 M ammonium
592 acetate; 0.02 M sodium citrate tribasic dihydrate; 0.02M potassium sodium tartrate

593 tetrahydrate; 0.02 M sodium oxamate; 0.10 M Tris-base [pH 8.5]; BICINE; 20% (v/v)
594 ethylene glycol; 10 % (w/v) PEG 8000).
595
596 The crystals were harvested in a nylon loop, flash-cooled and stored in liquid nitrogen
597 for data collection. Crystals were screened on beamlines Proxima-1 and Proxima-2 at
598 Synchrotron Soleil (Gif-sur-Yvettes, France) as well as beamlines I03 and I04-1 at
599 Diamond Light Source (Didcot, UK). Data for structure determination were collected on
600 the Proxima-2 beam-line at Synchrotron Soleil at a wavelength of 1.77 Å. Data were
601 indexed and integrated using XDS [37], scaled using XSCALE [37] and anisotropically
602 corrected using STARANISO, applying a high resolution cutoff of $I/\sigma I = 1.2$ [38]. The
603 crystals belong to space group C2, with the unit cell dimensions a=158.84, b=142.5300,
604 c=116.4200 $Å^3$ and β=102.61°. The structure was determined by molecular replacement
605 using Phaser [39], with the globular domain of RcsF (residues 51-130, PDB:2Y1B) and
606 the inward open BamA β-barrel (residues 422-809, PDB: 5D0O) and BamA POTRA
607 domain 4 (residues 265-344; PDB: 5D0O) as search models. Molecular replacement
608 searches identified two copies each of the BamA β-barrel, RcsF and POTRA domain 4.
609 Following 10 cycles of rigid body refinement POTRA domains 1, 2, 3 and 5 of the first
610 BamA-RcsF copy in the asymmetric unit (Extended Data Figure 2) could be manually
611 placed in the 2FoFc and FoFc difference density and were subjected to an additional 10
612 rounds of rigid body refinement. The model was refined to 3.8 Å resolution using
613 BUSTER [40] and intermittent manual inspection and correction of the model in Coot [41].
614 BUSTER was run using Local Structure Similarity Restraints (LSSR) over the two
615 copies in the asymmetric unit, as well as target-based similarity restraints using the
616 inward open BamA structure as reported in PDB:5D0O. The final model shows R and
617 freeR factors of 28.3% and 31.4%, respectively, containing 1388 amino acids, of which

618 19 are indicated as Ramachandran outliers (1.4%). We note that side chain positioning
619 is frequently ambiguous at 3.8 Å resolution and should therefore not be over-interpreted
620 by users of the deposited model. Side chains for which no unambiguous electron density
621 was observed were not pruned for ease of model interpretation. Such side chains were
622 included in refinement and manually modelled in there most likely rotamer using Coot.
623 Data collection and refinement statistics are found in Supplementary Table 1.
624

625 **Site-specific photo-crosslinking**

626 We used a site-specific photo-crosslinking method described previously [10] with some
627 modifications. To incorporate DiZPK into BamA, we used the pSup-Mb-DIZPK-RS
628 plasmid encoding an evolved *Methanosarcina barkeri* pyrrolysyl-tRNA synthetase and
629 an optimized $\mathrm{tRNA}_{\mathrm{CUA}}^{\mathrm{Pyl}}$ suppressor [24]. DH300 cells were co-transformed with pSup-Mb-
630 DIZPK-RS and one of the plasmids containing an amber codon in BamA in pSC270.
631 Cells were grown in 3-(N-morpholino) propanesulfonic acid (MOPS) minimal medium
632 supplemented with 0.2% glucose, 0.2% (w/v) arabinose, 200 μM IPTG, 0.001% (w/v)
633 casamino acids, and 0.8 mM DiZPK. When cells reached OD_{600} = 1, 500-μL samples
634 were irradiated with ultraviolet light at 365 nm or left unirradiated for 10 min. Cells
635 were precipitated with trichloroacetic acid, washed with ethanol, and proteins were
636 solubilized in 100 μL SDS-PAGE sample buffer (50 mM Tris-HCl [pH 7.5], 1% (w/v)
637 SDS, 10% (v/v) glycerol, 0.002% (w/v) bromophenol blue) before SDS-PAGE and
638 immunoblotting using anti-RcsF and anti-BamA antibodies.
639

640 ***In vivo* BS3 crosslinking**

641 Cells were harvested around mid-log phase (OD_{600} = ~ 0.5). *In vivo* crosslinking was
642 performed as described previously [10], except that bis(sulfosuccinimidyl)suberate
643 (CovaChem) was used instead of 3,3'-dithiobis(sulfosuccinimidyl propionate).
644

645 **Chemical crosslinking-mass spectrometry**

646 We first performed buffer exchange of the purified BamAB-RcsF complex using a PD-
647 10 desalting column (GE Healthcare Life Sciences). The complex was eluted with 20
648 mM HEPES [pH 7.5], 150 mM NaCl, and 0.1% (w/v) DDM. A 30-fold molar excess of
649 the crosslinker disuccinimidyl dibutyric urea (50 mM stock solution in dimethyl
650 sulfoxide, Thermo Scientific) was added to the protein solution and incubated at 37 °C
651 for 1 h. The reaction was quenched by adding Tris-HCl to a final concentration of 20
652 mM. Crosslinked proteins were precipitated with ethanol and trypsinized, and
653 crosslinked peptides were enriched through cation exchange as described previously [42].
654 Briefly, crosslinked proteins (50 µL) were precipitated by adding ice-cold ethanol (150
655 µL) and 3 M sodium acetate [pH 5.3] (5 µL) prior to incubation at −20 °C for 16 h. The
656 sample was centrifuged (16,200 x *g*, 4 °C, 30 min), the supernatant was removed, and
657 the pellet was washed by adding 80% (v/v) ice-cold ethanol (200 µL) and vortexing for
658 30 s. The sample was centrifuged again, the supernatant was removed, and the pellet
659 was dried in a vacuum centrifuge. The pellet was dissolved in 1% (w/v) RapiGest
660 (Waters) (10 µL) and trypsin (Sequencing grade, Promega) solution was added (90 µL,
661 1:50 trypsin:protein mass ratio) before incubating overnight at 37 °C. Trifluoroacetic
662 acid was added (final concentration 0.5% (v/v)) and the sample was incubated at 37 °C
663 for 1 h to precipitate the Rapigest. The mixture was centrifuged (16,200 x *g*, 4 °C, 30
664 min), the supernatant was concentrated using a vacuum centrifuge, and the pellet was
665 dissolved in 20% (v/v) acetonitrile/0.4% (v/v) formic acid (20 µL). Strong cation

666 exchange enrichment was carried out using OMIX 10 µL strong cation exchange pipette
667 tips (Agilent) as previously described [42].
668
669 Fractionated peptides (5 µL) were injected onto a reverse-phase Acquity M-Class C18,
670 75 µm x 150 mm column (Waters) and separated via gradient elution of 1-50% (v/v)
671 solvent B (0.1 % (v/v) formic acid in acetonitrile) in solvent A (0.1 % (v/v) formic acid
672 in water) over 60 min at 300 nL/min. The eluate was infused into a Xevo G2-XS
673 (Waters) mass spectrometer operating in positive ion mode. Mass calibration was
674 performed by infusion of aqueous NaI (2 µg/µL). [Glu1]-Fibrinopeptide B was used for
675 the lock mass spray, with a 0.5 s lock spray scan taken every 30 s. The lock mass
676 correction factor was determined by averaging 10 scans. Data acquisition was
677 performed in DDA mode with a 1 s mass-spectrometry scan over *m*/*z* 350-2000.
678 Instrument parameters were optimized for the detection of crosslinked peptides, as
679 described previously [43]. Data processing and crosslink identification were performed
680 using MeroX [44].
681
682 **Expression of BamA mutants and co-purification with RcsF**
683 pBamA and pBamA-B each provide chromosomal-level expression of BamA [10].
684 Therefore, we introduced mutations of *bamA* in these plasmids to test the physiological
685 effects of BamA mutants; plasmids were expressed in the presence or absence of *bamA*
686 on the chromosome. Cells (2 mL) were harvested at OD_{600} ~ 0.5 to purify BamA,
687 except during the following experiment. The cysteine mutants of BamA, when oxidized
688 to form a disulfide bond, allow BamA to form an "open" or "closed" lateral gate.
689 Therefore, the efficiency of disulfide-bond formation in these mutants is very important.
690 To enhance the oxidation of cysteines to form disulfide bonds, we added 3 mM

691 tetrathionate as an oxidant [45] at OD_{600} ~ 0.5 and harvested cells (1 mL) at OD_{600} ~ 1.0.

692

693 Since there was a six-histidine tag at the N-terminus of BamA, we used Dynabeads™
694 His-Tag (Invitrogen) for Ni-affinity purification. After resuspending cells in 350 μL of
695 25 mM Tris-HCl [pH 7.4], 290 mM NaCl, 1 mM imidazole, and 0.05% (w/v) DDM
696 (buffer A), cells were lysed via mild sonication on ice. Membrane vesicles were further
697 solubilized by increasing the DDM concentration to 1% (w/v). After removing debris
698 via centrifugation at 9,300 × *g* for 10 min, 5 μL of Dynabeads™ His-Tag (pre-washed
699 with buffer A and resuspended in the same volume) were added to 250 μL of the
700 supernatant, which was incubated for 20 min at 4 °C. The rest of the supernatant was
701 used as the input fraction. The magnetic beads were pulled by a magnet and the
702 supernatant was taken for the flow-through fraction. After washing the beads three
703 times with 750 μL buffer E using the magnet, bound proteins were eluted with 83 μL
704 (three times enrichment compared to the other fractions) of buffer A with 300 mM
705 imidazole. Forty microliters of the input, flow-through, and elution fractions were
706 mixed with SDS-PAGE sample buffer. After denaturation of the three fractions, SDS-
707 PAGE was performed, followed by immunoblotting using rabbit-raised anti-BamA,
708 anti-RcsF [10], anti-BamB, anti-BamC, anti-BamD, and anti-BamE.

709

710 To determine the redox states of the cysteine-introduced gate mutants of BamA, we
711 added 3 mM N-ethylmaleimide in SDS-PAGE sample buffer to alkylate cysteines to
712 prevent thiol-disulfide exchange. The sample was divided into two aliquots and 10 mM
713 of tris(2-carboxyethyl) phosphine was added to one of them to obtain the reduced state
714 of BamA as a control. Nu-PAGE (4-12% gradient; Novex) was used to separate the
715 oxidized and reduced bands of BamA.

716

717 **Spotting assay for growth.** Cells were grown in M9 minimal glucose medium at 30°C
718 until they reached OD_{600} =1. Tenfold serial dilutions were made in M9 minimal
719 glucose, plated onto M9 minimal glucose or LB agar, and incubated at 30°C or 37°C.
720 Plates were supplemented with ampicillin (200 µg/ml).

721

722 **Biolayer interferometry**

723 Untagged BamA was first biotinylated using the EZ-Link NHS-PEG4-biotin kit (Perbio
724 Science). The reaction was stopped by adding Tris [pH 8] to the final concentration of
725 20 mM. Excess NHS-PEG4-biotin was removed by passing the sample through a Zeba
726 Spin Desalting column (Perbio Science). Biolayer interferometry was performed in
727 black 96-well plates (Greiner) at 25 °C using OctetRed96 (ForteBio). Streptavidin and
728 Ni-NTA biosensor tips (ForteBio) were hydrated with 0.2 mL working buffer (20 mM
729 Tris [pH 8], 150 mM NaCl, 0.03 % (w/v) DDM) and then loaded with biotinylated
730 BamA or 6xHis-tagged RcsF, respectively.

731

732 In the forward experiment, purified 6xHis-tagged RcsF (5 µg/mL) was immobilized on
733 Ni-NTA sensors until the signal reached 0.5-0.6 nm. Association and dissociation of
734 BamA to RcsF-coated tips were monitored for 1200 s and 300 s, respectively, by
735 dipping tips into BamA-containing buffer (serial two-fold dilution from 4000 nM to
736 62.5 nM), and subsequently in buffer only. In the reverse experiment, biotinylated
737 BamA was immobilized on streptavidin sensor tips to a signal of 2.0 nm. The
738 association and dissociation of RcsF (serial 3-fold dilution from 3000 nM to 12.34 nM)
739 to BamA-coated tips were monitored for 4800 s and 700 s, respectively. Dissociation

740 constants were determined using Graphpad Prism by linear regression of the steady-
741 state binding responses in the saturation binding experiment (Extended Data Fig. 4c, d).
742
743 For binding of the BamA$^{G393C/G584C}$ mutant (Extended Data Fig. 5c), 6xHis-tagged RcsF
744 was immobilized on Ni-NTA sensors. To follow BamA association and dissociation,
745 RcsF-coated tips were dipped into 0.2 mL of 200 nM BamA solution, with or without 2
746 mM diothiothreitol, for 1200 s, followed by 1200 s in buffer only.
747
748 **Antibodies and immunoblotting**
749 Rabbit anti-RcsF antibody was previously generated and used by us [10]. We newly raised
750 the antibodies against BamA, BamB, BamC, BamD, and BamE in rabbits as follows.
751 Except BamA, the DNA sequences encoding the proteins without the signal sequence
752 were cloned into pET28a (Novagen) using the NcoI and XhoI restriction sites, which
753 allows the expressed proteins to be his-tagged at the C-terminus. For BamA, DNA
754 encoding the POTRA domains (1-4) of BamA with a C-terminal strep-tag (but without
755 the signal sequence) was cloned in pET21a (Novagen). All the proteins above were
756 overexpressed in BL21(DE3) and purified using standard methods for Ni-NTA affinity
757 purification or streptavidin purification (POTRA 1-4). Small aliquots of the purified
758 proteins were sent to the CER group (Marloie, Belgium) to raise antibodies in rabbits.
759 Goat Anti-Rabbit IgG alkaline phosphatase conjugated (Sigma) was used as a secondary
760 antibody at a 1:20,000 dilution.
761
762 Antibody specificity was confirmed by comparing the immunoblot of the wild-type
763 strain with that of a mutant using each corresponding antibody. The dilutions of the
764 antibodies for immunoblotting were 1:10,000 (BamA), 1:20,000 (BamB), 1:40.000

765 (BamC), 1:10,000 (BamD), and 1:20,000 (BamE). The specificity of the antibodies was
766 verified; data are available upon request.
767
768 To simplify the detection of Bam components and RcsF after purification of BamA, we
769 used two mixtures of antibodies (anti-BamA plus anti-RcsF; anti-BamB, anti-BamC,
770 anti-BamD, plus anti-BamE). Detection specificity was verified using similar mutants
771 as above but harboring pBamA. Data are available upon request.
772
773 The antibody recognizing the transmembrane domain of OmpA is a gift from the
774 Bernstein laboratory [46]. The rabbit polyclonal OmpC antibody was purchased from
775 EPIGENTEK. The anti-*E. coli* EF-Tu antibody (mAb 900) was purchased from
776 HycultBiotech. The Goat anti-mouse IgG conjugated with the Cy3 fluorescent dye was
777 used as a secondary antibody for EF-Tu (Amersham).
778
779 **β-galactosidase assay**
780 Rcs induction was monitored by measuring β-galactosidase activity as described [47].
781 Briefly, cells harboring P*rprA-lacZ* at the *att*B phage lambda site on the chromosome
782 were diluted 1:100 from overnight cultures in Luria broth (LB), then incubated at 37°C.
783 Cells were harvested at OD_{600} = 0.6-1. Twenty microliters of cells were harvested and
784 incubated with 80 μl of permeabilization solution (60 mM $Na_2HPO_4 \cdot 2H_2O$, 40 mM
785 $NaH_2PO_4 \cdot H_2O$, 10 mM KCl, 1 mM $MgSO_4 \cdot 7H_2O$, 50 mM β-mercaptoethanol) for 30–
786 45 min at room temperature. Then, 600 μl of substrate (1 mg/ml O-nitrophenyl-β-d-
787 galactoside, 50 mM β-mercaptoethanol) were added. The mixture was further incubated
788 at 30°C for 20-90 min. Seven hundred microliters of 1 M Na_2CO_3 were added to stop
789 the reaction, and the optical density was measured at 420 nm. The standardized amount

790 of β-galactosidase activity was reported in Miller units. The ratio of P*rprA-*
791 *lacZ* induction was calculated relative to the basal level in a WT strain. Bar graphs with
792 corresponding statistical analysis were prepared using Prism 7 (GraphPad Software,
793 Inc.).
794
795 **Statistical methods**
796 The significance of differences among bacterial strains was assessed using GraphPad
797 Prism 8 according to analysis of variance (two ways ANOVA), followed by the
798 application of Tukey's multiple-comparison test. Normality was assessed using the
799 Shapiro-Wilk test.
800
801 **Molecular modeling: protein insertion in the lipid bilayer**
802 The initial simulation system was prepared starting from the BamA-RcsF complex
803 determined in this work (PDB code 6T1W) with the POTRA1-4 domains removed.
804 Missing residues and C-terminal residues of BamA and RcsF were completed with
805 MODELLER v9.22 [48] to generate a protein complex containing residues 347-810 for
806 BamA and 51-134 for RcsF. This complex was preorientated with respect to the
807 membrane normal (*z* axis) using the structure 5AYW [6] from the OPM database
808 (https://opm.phar.umich.edu) [49] as template, then embedded in an asymmetric bilayer to
809 mimic the *E. coli* outer membrane using CHARMM-GUI (http://www.charmm-gui.org)
810 [50] and following the protocols described for OmpLA [51] and BamA [52]). The inner leaflet
811 was a mixture of 100 lipids: 75 1-palmitoyl(16:0)-2-palmitoleoyl(16:1 *cis*-9)-
812 phosphatidylethanolamine (PPPE), 20 1-palmitoyl(16:0)-2-vacenoyl(18:1 *cis*-11)-
813 phosphatidylglycerol (PVPG), and 5 1,10-palmitoyl-2,20-vacenoyl cardiolipin with a
814 net charge of –2e (PVCL2), corresponding to a ratio of 15:4:1. The outer leaflet was

815 composed of 36 LPS (including the lipid A, R1 core and O-antigen polysaccharide
816 fragments). The equilibration was performed according to the standard protocol from
817 CHARMM-GUI Membrane Builder, with restraints that were gradually reduced in 6
818 steps (2.125 ns overall), using CHARMM version 44b1 [53]. A similar protocol was used
819 to build a second system, containing the outward-open conformation of BamA (PDB
820 code 5D0Q) [5] with the POTRA1-4 domains removed and the RcsF from 6T1W shifted
821 upwards on the *z* axis by 30 Å.
822
823 **Dynamic importance sampling simulations**
824 Dynamic importance sampling (DIMS) uses a biasing with correction approach to
825 improve the sampling efficiency of rare events. The *soft ratcheting* algorithm generates
826 transitions between states using a stochastic approach [54]. It should be noted that at any
827 point of the DIMS simulation the intermediate system is realistic (no force is applied
828 and the potential function is not modified) and the simulated pathway is always
829 possible, although it may not be in all cases the lowest energy one. In this work, we
830 carried out DIMS Langevin dynamics (LD) simulations using CHARMM version 44b1
831 (collision frequency of 25.0) starting from the first system and with the second system
832 as target. The "soft-ratcheting" implemented in DIMS accepts all steps proceeding
833 towards the desired final state and a fraction of steps away from the target. This fraction
834 is defined by DIMS-Cartesian for which we used the recommended value of 10^{-6} [55].
835 Two replicas were simulated, providing similar results, and only the results from the
836 first replica are presented here.
837
838 **Image and video rendering**

The pictures representing molecular data were generated using PyMOL version 2.2.0 (Schrödinger LLC, https://pymol.org). The video was generated from the DIMS simulation (replica 1) using VMD [56].

842 **LEGENDS TO EXTENDED DATA FIGURES**

843

844 **Extended Data Figure 1. RcsF can be co-purified with the BAM complex. (a,b,c)**
845 Gel filtration profiles of the affinity-purified BamAB-RcsF, BAM-RcsF and BAM
846 complexes. The size exclusion chromatography was performed using a HiLoad 10/300
847 Superdex 200pg. The input and peak fractions were collected and the samples were
848 analyzed by blue native electrophoresis with Coomassie staining. The migration pattern
849 of BamABCDE-RcsF (b) was modified compared to BamABCDE (c) upon size
850 exclusion chromatography (band 8 increases), reflecting the higher instability of the
851 BamABCDE-RcsF complex. n= 4 biologically independent experiments.

852

853 **Extended Data Figure 2. Crystal structure of the BamA-RcsF complex. (a, b)** Final
854 2Fo-Fc electron map of the BamA-RcsF complex, shown with a map contour level of
855 0.08 e-/Å^3 (root mean square deviation 1.02 Å). The asymmetric unit of the crystals
856 holds two BamA-RcsF copies, one revealing interpretable electron density for the full
857 BamA sequence (a), and a second revealing unambiguous density for POTRA domain 4
858 only (b). In the second copy (b), the electron density corresponding to POTRA domains
859 1, 2, 3, and 5 is too weak to allow unambiguous rigid body placement of the domains.
860 All descriptions and images in the main text are based on the first copy (a). **(c)** Overlay
861 of two BamA-RcsF complexes in the asymmetric unit. The first complex depicts BamA
862 in gold and RcsF in blue, while these molecules are yellow and light blue, respectively,
863 in the second complex. In both copies, RcsF makes an average displacement of 4 Å
864 relative to the BamA β-barrel. (**d**) Crystal packing of the BamA-RcsF complex viewed
865 along the a- (left) and c-axis (right). For the first copy of the BamA-RcsF complex in
866 the asymmetric unit (orange-slate) the conformation of the POTRA domains is

867 stabilized by the packing along the b-axis, whilst for the second copy (cyan-slate) only
868 POTRA domain 4 is involved in crystal contacts. In the latter, POTRA 5, 3, 2 and 1 are
869 not in contact with neighboring molecules and show weak electron density only due to
870 the lack of conformational stabilization.
871
872 **Extended Data Figure 3. Structural dynamics of the BamA POTRA domains. (a,**
873 **b)** Superimposition of BamA-RcsF (gold and blue, respectively) with the POTRA
874 domains in the inward-open BamABCDE complex (PDB: 5D0O; light blue) or the
875 outward-open BamACDE complex (PDB: 5EKQ; green). Complexes are superimposed
876 based on 400 equivalent Cα atoms in the BamAβ-barrel, and shown in side (a) or
877 periplasmic (b) view. For 5d0o and 5ekq, the accessory Bam subunits and the BamA β-
878 barrel are omitted for clarity. **(c)** Periplasmic view of the inward-open BamABCDE
879 complex, showing binding of the BAM accessory proteins BamB (magenta), BamC
880 (red), BamD (blue), and BamE (yellow). Pulldown experiments showed that RcsF binds
881 the BamABCDE complex (Fig. 1). In agreement with this observation, structural
882 comparisons reveal that RcsF binding would not result in direct steric clashes with any
883 BAM accessory protein. However, the positions of the POTRA domains in the BamA-
884 RcsF and BamABCDE complexes are markedly different. In the BamA-RcsF complex,
885 POTRA5 makes a 26° outward rotation to accommodate RcsF (see also Fig. 3), and a
886 reorganization in the joint between POTRA domains 3 and 2 results in a more extended
887 conformation of the POTRA "arm" and the projection of POTRA domains 2 and 1
888 further from the BamA β-barrel, a conformation not previously reported in available
889 BamA structures. In the BamABCDE complex, BamD contacts both POTRA5 and the
890 joint of POTRA domains 1 and 2. In the BamA-RcsF complex, POTRA5 and POTRA
891 domains 2 and 1 are too distant to be bridged by BamD; binding of BamD to BamA-

892 RcsF therefore requires a conformational change in the POTRA arm or the dissociation
893 of BamD at either of these two contact points.
894
895 **Extended Data Figure 4. Validation of the BamA-RcsF structure.** (**a**) RcsF
896 aminoacid sequence. The sequence coverage of the XL-MS experiment was about 60%
897 as highlighted in violet (**b**) Ribbon diagram of the BamA-RcsF structure. Highlighted
898 residues show sites mutated to amber for incorporation of the photoreactive lysine
899 analog DiZPK. Sites that crosslink to RcsF are green, sites that show no crosslinking are
900 magenta. Mutation of extracellular loop 1 (^{e}L1; red) leads to loss of RcsF binding (see
901 panel g). BamA sidechains found to crosslink with RcsF by means of the
902 homobifunctional amine-reactive crosslinker disuccinimidyl dibutyric urea (DSBU) are
903 shown as sticks and colored cyan. Residue K61 from RcsF, which was found to
904 crosslink to BamA using DSBU, is shown as a stick and colored orange. The other two
905 RcsF residues (K42 and K134) that could be crosslinked to BamA are not visible in this
906 structural model. (**c**) *In vivo* photocrosslinking experiment in which cells expressing the
907 BamA mutants containing DiZPK at the indicated positions were treated (+) or not (-)
908 with ultraviolet light. Proteins samples were analyzed via SDS-PAGE and
909 immunoblotted with anti-RcsF or anti-BamA antibodies, showing that the photo-
910 crosslinked complexes contain BamA and RcsF. n= 3 biologically independent
911 experiment. WT, wild type. (**d, e**) Sensorgrams from biolayer interferometry (n=1) (left)
912 and corresponding equilibrium binding plots (right) of immobilized RcsF titrated with
913 BamA (d) or immobilized BamA titrated with RcsF (e). (**f**) The levels of major OMPs
914 are slightly decreased in cells expressing $BamA_{\Delta loop1}$. WT cells harboring the empty
915 plasmid (pAM238) were used as control and EF-Tu expression levels were analyzed as
916 loading control. n= 3 biologically independent experiments. (**g**) Deletion of loop 1 in

917 BamA prevents RcsF from being pulled down with BamA. WT cells harboring the
918 empty plasmid (pAM238) were used as control. n= 3 biologically independent
919 experiments. (**h**) Overexpression of pBamA$_{\Delta Loop1}$ in a *bamA* deletion strain activates the
920 Rcs system compared to WT. A chromosomal *rprA::lacZ* fusion was used to monitor
921 Rcs activity, and specific β-galactosidase activity was measured from cells at mid-log
922 phase (OD_{600}=0.5). Boxplot with whiskers (median, first and third percentiles, lower
923 and upper extreme) from minimum to maximum. All values were normalized to the
924 average activity obtained for WT cells harboring the empty plasmid (pET3a) obtained
925 from n= 8 biologically independent experiments. WT, wild type; Kan, kanamycin.
926
927 **Extended Data Figure 5. RcsF binds the inward-open conformation of BamA.** (**a**)
928 Models for the BamA$^{G393C/G584C}$ [5] and BamA$^{G433C/N805C}$ [26] double cysteine mutants,
929 which are locked in the outward-open or inward-open conformation, respectively, when
930 oxidized. Mutated cysteines are shown as atom spheres. (**b**) BamA barrel locking and
931 RcsF binding. Overexpression of double cysteine mutants pBamA$^{G393C/G584C}$-B and
932 BamA$^{G433C/N805C}$-B in a wild-type strain. RcsF can be co-purified with the BamA β-
933 barrel locked in the inward-open conformation (BamA$^{G433C/N805C}$) by a disulfide bond
934 (ox) but not in the outward-open conformation (BamA$^{G393C/G584C}$). BamA mutants
935 become reduced (red) following treatment with tris(2-carboxyethyl) phosphine (TCEP)
936 and migrate similarly. The oxidized form of BamA$^{G393C/G584C}$ migrates more slowly than
937 wild-type BamA. As a result, two bands are visible for BamA in the input of
938 BamA$^{G393C/G584C}$, the lower migrating band corresponding to wild-type BamA expressed
939 from the chromosome. n= 3 biologically independent experiments. (**c**) Sensorgram
940 from biolayer interferometry of immobilized RcsF titrated with BamA$^{G393C/G584C}$,
941 without (oxidized; - DTT) or with dithiothreitol (reduced; + DTT). When the β-barrel is

942 locked in the outward-open conformation (-DTT), RcsF is unable to bind BamA. When
943 reduced, $BamA^{G393C/G584C}$ regains binding, demonstrating that BamA reverts to the
944 inward-open conformation in which it can bind RcsF.
945
946 **Extended Data Figure 6. The movement of POTRA5 towards the periplasmic exit**
947 **of the lumen of the BamA barrel could push RcsF upwards.** (**a, b**) Lateral view of
948 the initial and final conformations, respectively, of the BamA-RcsF complex during the
949 dynamic importance sampling simulation (DIMS) of the BamA-RcsF complex. (**c, d**)
950 Bottom view (from the periplasm) of the above conformations. BamA and RcsF are
951 colored in orange and blue, respectively. The initial conformation of the system (BamA
952 and RcsF) corresponds to the structure determined in this work (PDB code 6T1W) [5]
953 with the POTRA1-4 domains removed. The final conformation of BamA is similar to
954 the outward-open structure (PDB code 5D0Q). The explicit outer membrane and solvent
955 are not shown for clarity. (**e**) Expression from $BamA^{hinge}$ from a plasmid in Δ*bamA* cells
956 leads to a severe growth defect when cells are grown at 37°C in rich media, but not
957 when they are grown in minimal media at 30°C. Cells were grown in M9 minimal
958 glucose medium at 30°C until they reached OD_{600} =1. Tenfold serial dilutions were
959 made in M9 minimal glucose, plated onto M9 minimal glucose or LB agar, and
960 incubated at 30°C or 37°C. Plates were supplemented with ampicillin (200 μg/ml). n=3
961 biologically independent experiments.

REFERENCES

34 Yu, D. *et al.* An efficient recombination system for chromosome engineering in Escherichia coli. *Proc Natl Acad Sci U S A* **97**, 5978-5983, doi:10.1073/pnas.100127597 (2000).

35 Koskiniemi, S., Pranting, M., Gullberg, E., Nasvall, J. & Andersson, D. I. Activation of cryptic aminoglycoside resistance in Salmonella enterica. *Mol Microbiol* **80**, 1464-1478, doi:10.1111/j.1365-2958.2011.07657.x (2011).

36 Roman-Hernandez, G., Peterson, J. H. & Bernstein, H. D. Reconstitution of bacterial autotransporter assembly using purified components. *Elife* **3**, e04234, doi:10.7554/eLife.04234 (2014).

37 Kabsch, W. Xds. *Acta Crystallogr D Biol Crystallogr* **66**, 125-132, doi:10.1107/S0907444909047337 (2010).

38 Tickle, I. J., Flensburg, C., Keller, P., Paciorek, W., Sharff, A., Vonrhein, C., Bricogne, G. . *STARANISO*, 2018).

39 McCoy, A. J., Grosse-Kunstleve, R.W., Adams, P.D., Winn, M.D., Storoni, L.C., & Read, R.J. Phaser crystallographic software. *J. Appl. Cryst.* **40**, 658-674 (2007).

40 Bricogne G., B. E., Brandl M., Flensburg C., Keller P., Paciorek W., & Roversi P, S. A., Smart O.S., Vonrhein C., Womack T.O. BUSTER version 2.10.3. (2017).

41 Emsley, P. & Cowtan, K. Coot: model-building tools for molecular graphics. *Acta Crystallogr D Biol Crystallogr* **60**, 2126-2132, doi:S0907444904019158 [pii] 10.1107/S0907444904019158 (2004).

42 Schmidt, C. & Robinson, C. V. A comparative cross-linking strategy to probe conformational changes in protein complexes. *Nat Protoc* **9**, 2224-2236, doi:10.1038/nprot.2014.144 (2014).

43 James, J. M. B., Cryar, A. & Thalassinos, K. Optimization Workflow for the Analysis of Cross-Linked Peptides Using a Quadrupole Time-of-Flight Mass Spectrometer. *Anal Chem* **91**, 1808-1814, doi:10.1021/acs.analchem.8b02319 (2019).

44 Iacobucci, C. *et al.* A cross-linking/mass spectrometry workflow based on MS-cleavable cross-linkers and the MeroX software for studying protein structures and protein-protein interactions. *Nat Protoc* **13**, 2864-2889, doi:10.1038/s41596-018-0068-8 (2018).

45 Osborne, A. R. & Rapoport, T. A. Protein translocation is mediated by oligomers of the SecY complex with one SecY copy forming the channel. *Cell* **129**, 97-110, doi:10.1016/j.cell.2007.02.036 (2007).

46 Hussain, S. & Bernstein, H. D. The Bam complex catalyzes efficient insertion of bacterial outer membrane proteins into membrane vesicles of variable lipid composition. *J Biol Chem* **293**, 2959-2973, doi:10.1074/jbc.RA117.000349 (2018).

47 Miller, J. C. *Experiments in Molecular Genetics*. (Cold Spring Harbor Laboratory Press, 1972).

48 Sali, A. & Blundell, T. L. Comparative protein modelling by satisfaction of spatial restraints. *J Mol Biol* **234**, 779-815, doi:10.1006/jmbi.1993.1626 (1993).

49 Lomize, M. A., Pogozheva, I. D., Joo, H., Mosberg, H. I. & Lomize, A. L. OPM database and PPM web server: resources for positioning of proteins in membranes. *Nucleic Acids Res* **40**, D370-376, doi:10.1093/nar/gkr703 (2012).

50 Lee, J. *et al.* CHARMM-GUI Membrane Builder for Complex Biological Membrane Simulations with Glycolipids and Lipoglycans. *J Chem Theory Comput* **15**, 775-786, doi:10.1021/acs.jctc.8b01066 (2019).

51 Wu, E. L. *et al.* E. coli outer membrane and interactions with OmpLA. *Biophys J* **106**, 2493-2502, doi:10.1016/j.bpj.2014.04.024 (2014).

52 Fleming, P. J. *et al.* BamA POTRA Domain Interacts with a Native Lipid Membrane Surface. *Biophys J* **110**, 2698-2709, doi:10.1016/j.bpj.2016.05.010 (2016).

53 Brooks, B. R. *et al.* CHARMM: the biomolecular simulation program. *J Comput Chem* **30**, 1545-1614, doi:10.1002/jcc.21287 (2009).

54 Perilla, J. R., Beckstein, O., Denning, E. J. & Woolf, T. B. Computing ensembles of transitions from stable states: Dynamic importance sampling. *J Comput Chem* **32**, 196-209, doi:10.1002/jcc.21564 (2011).

55 Denning, E. J. & Woolf, T. B. Cooperative nature of gating transitions in K(+) channels as seen from dynamic importance sampling calculations. *Proteins* **78**, 1105-1119, doi:10.1002/prot.22632 (2010).

56 Humphrey, W., Dalke, A. & Schulten, K. VMD: visual molecular dynamics. *J Mol Graph* **14**, 33-38, 27-38, doi:10.1016/0263-7855(96)00018-5 (1996).

Extended Data Figure 1

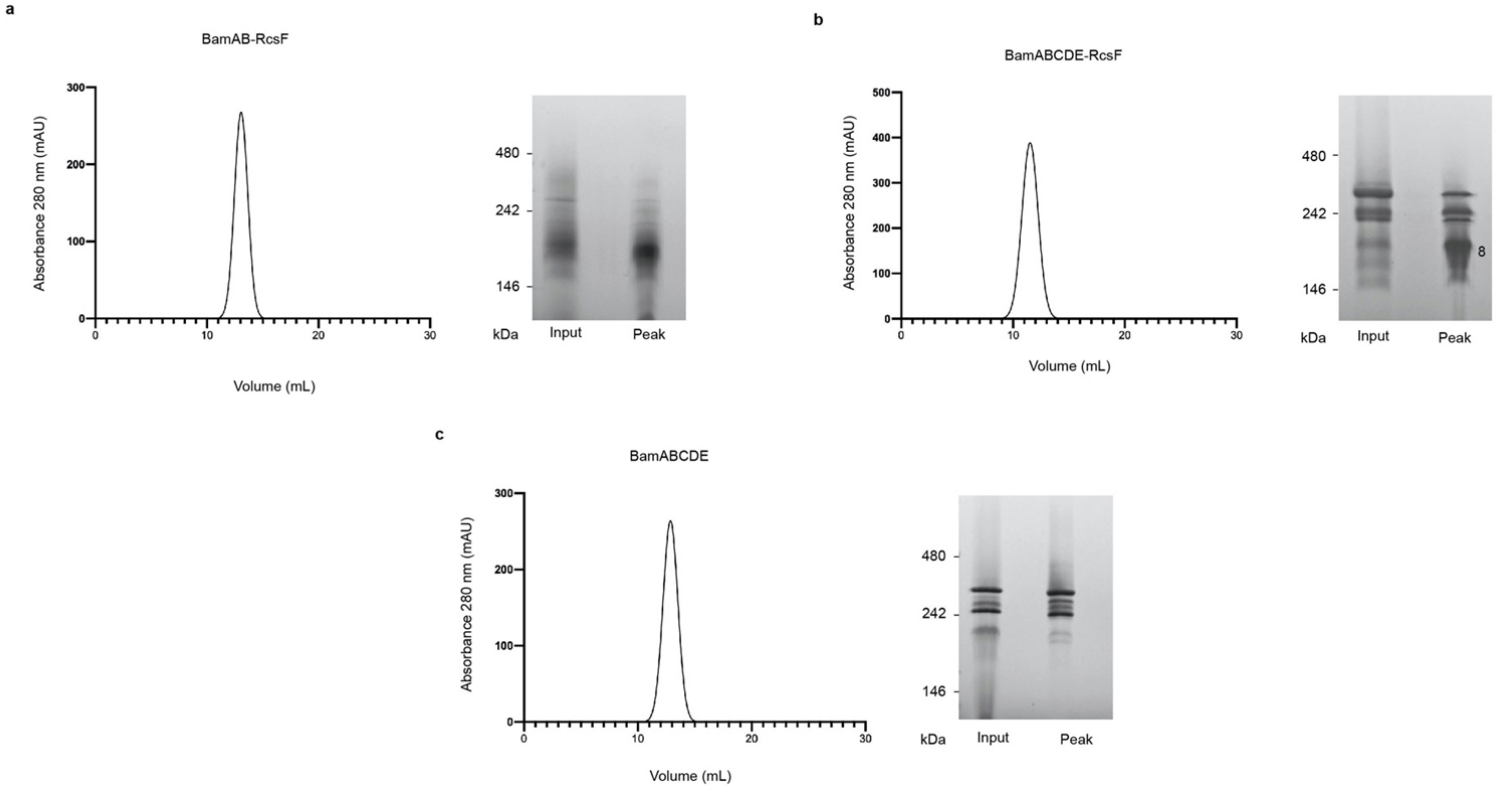

Extended Data Figure 2

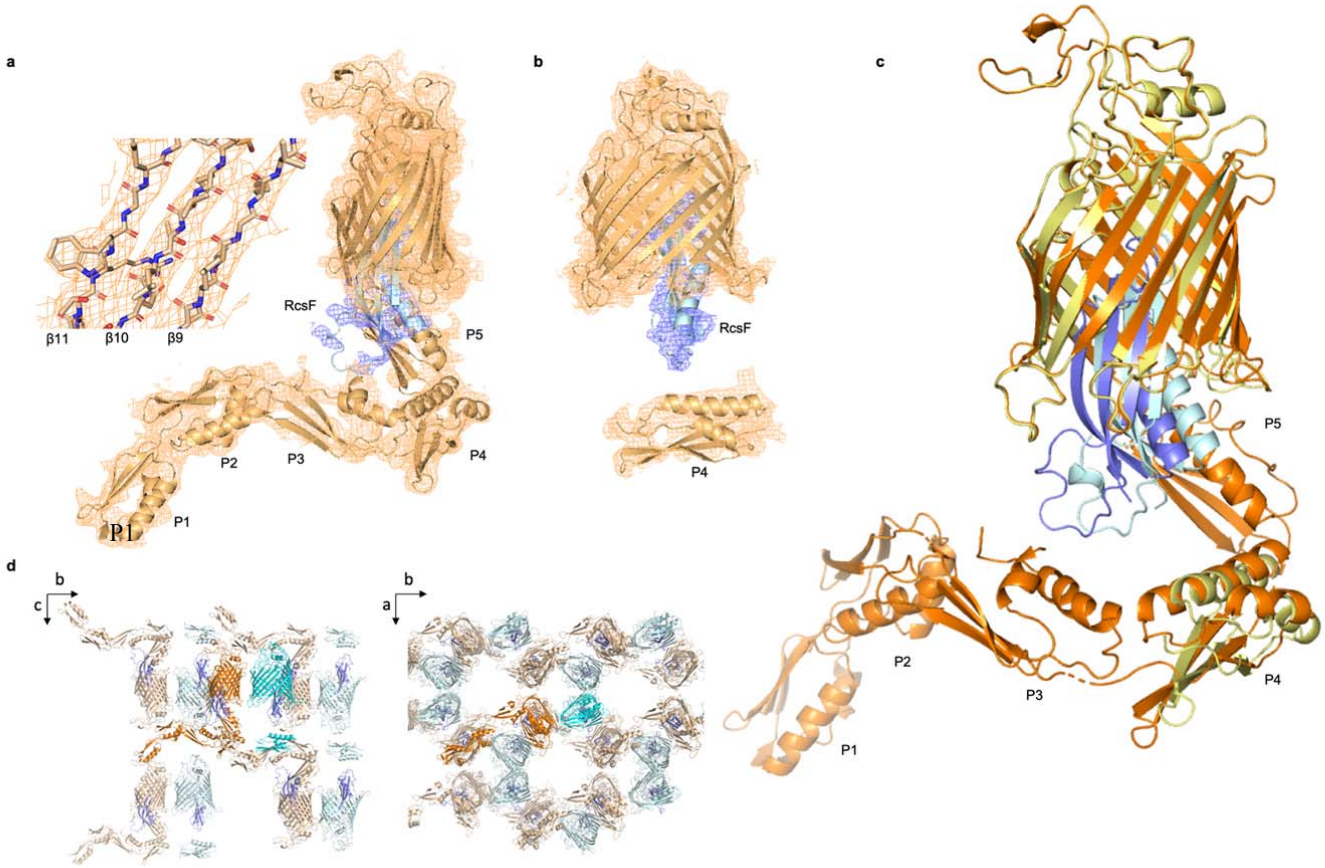

Extended Data Figure 3

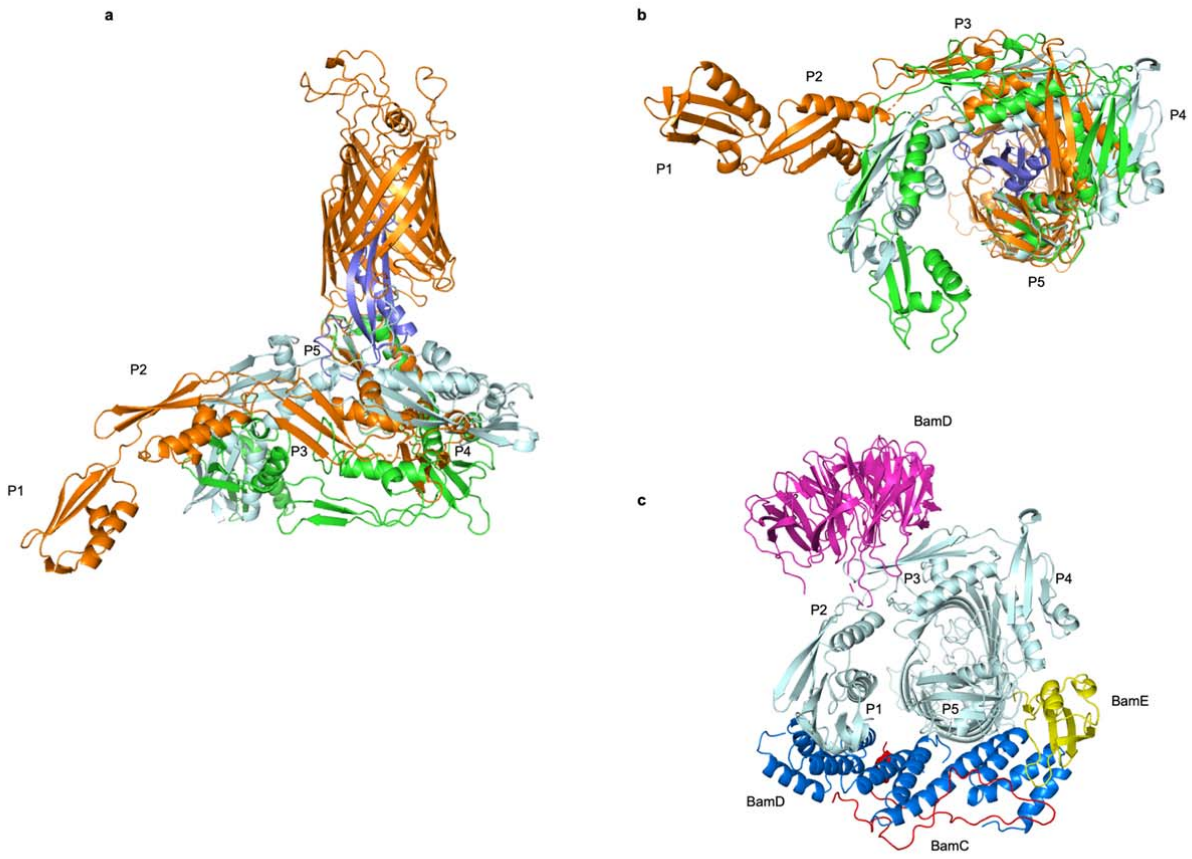

Extended Data Figure 4

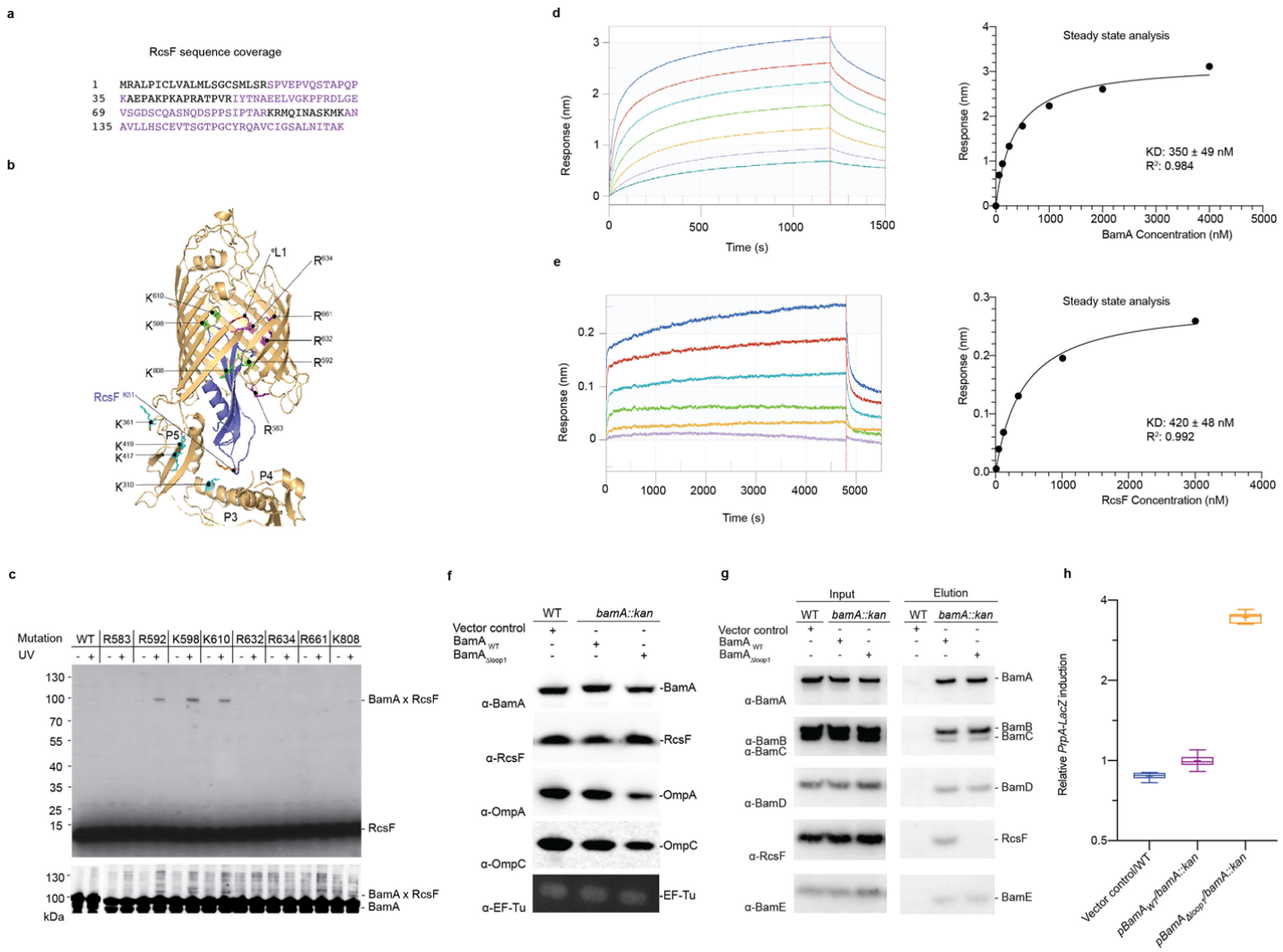

Extended Data Figure 5

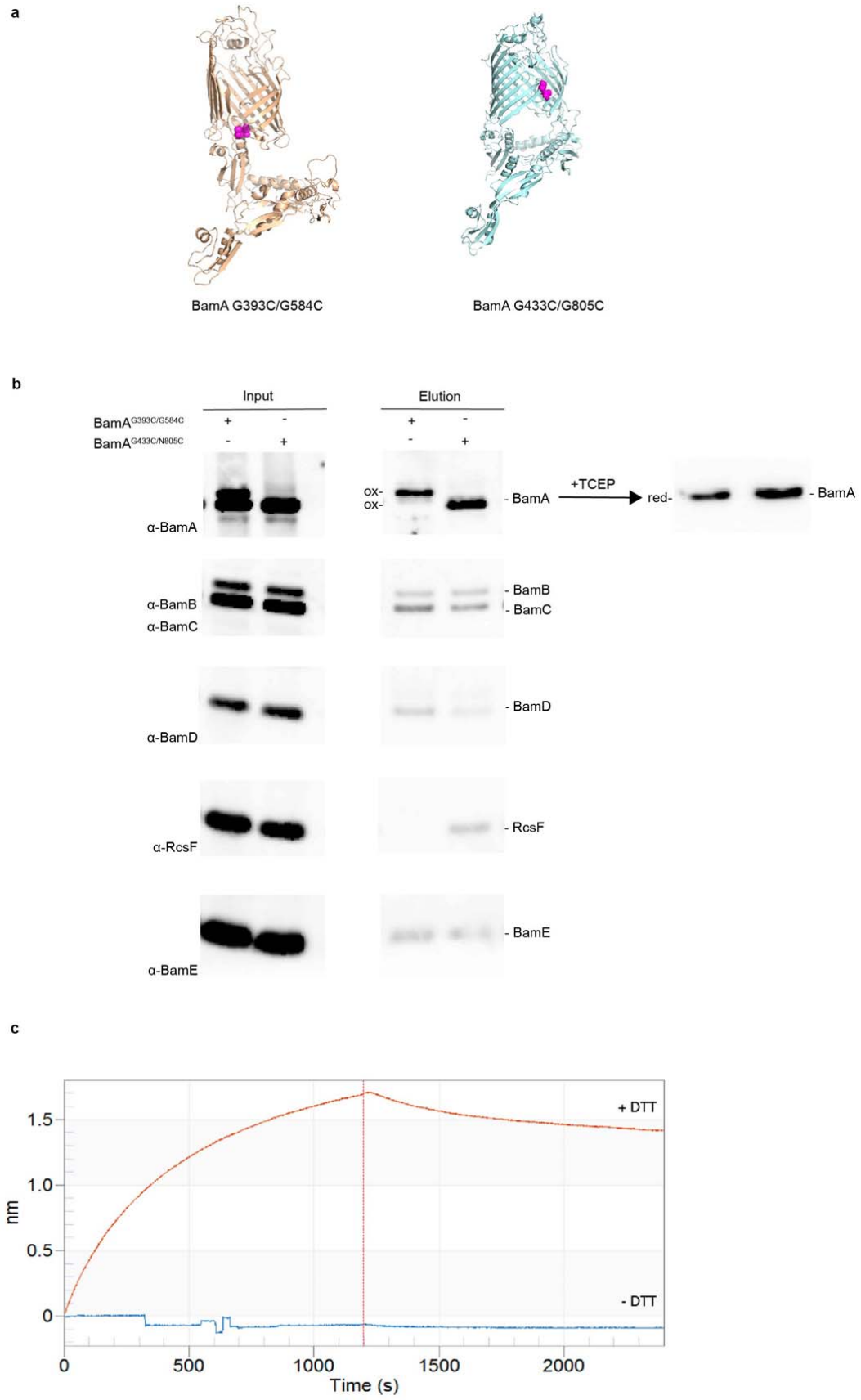

Extended Data Figure 6

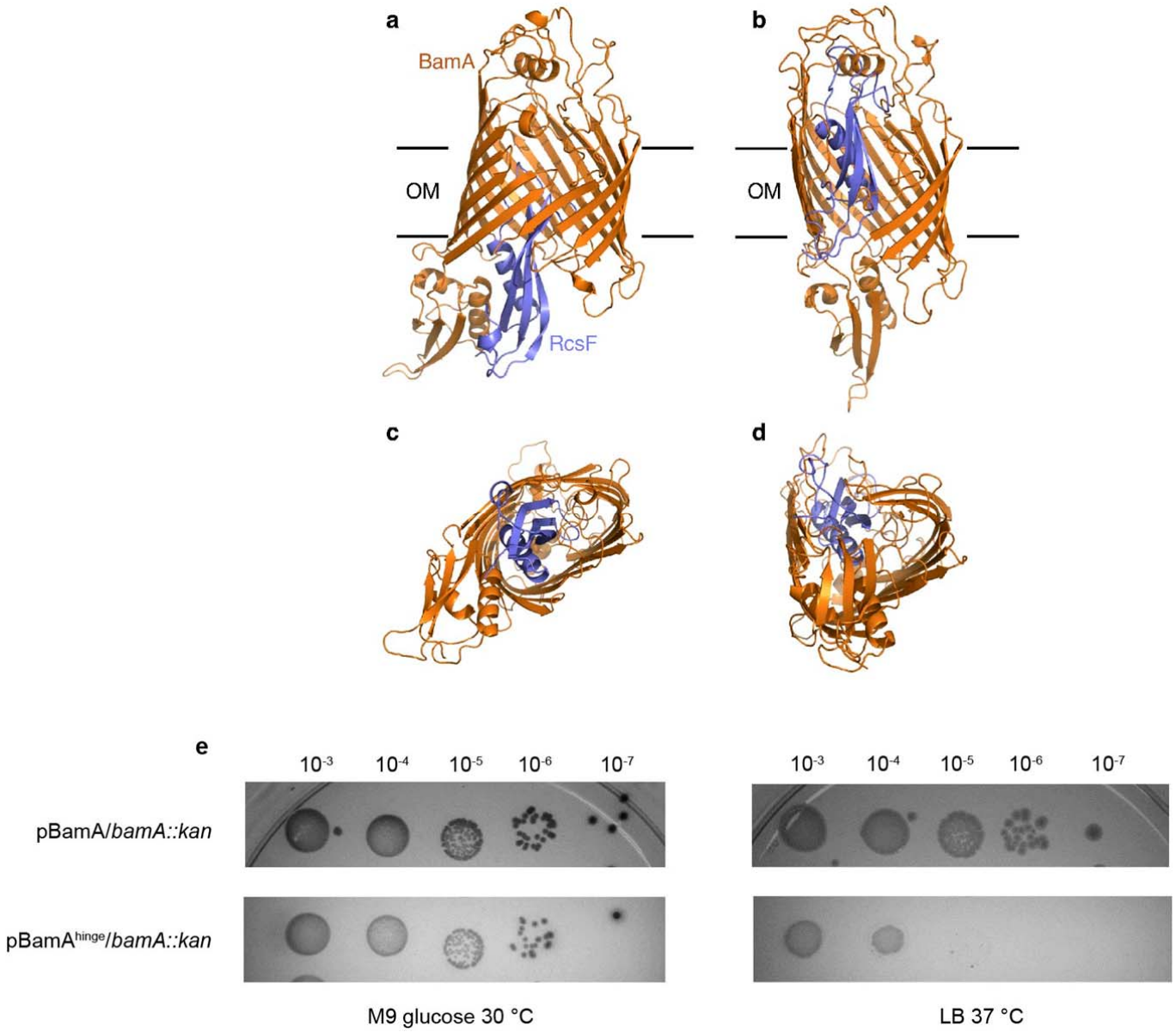

1028
1029
1030
1031
1032
1033
1034
1035
1036
1037
1038

1039 **Supplementary Information**

Supplementary Table 1. Data collection and refinement statistics.

	BamA-RcsF
Data collection	
Space group	C2
Cell dimensions	
a, *b*, *c* (Å)	158.84, 142.53, 116.42
α, β, γ (°)	90.0, 102.6, 90.0
Resolution (Å)**	48.6 – 3.8 (4.0 – 3.8) *
R_{pim}	0.02 (0.79)
$I / \sigma I$	15.9 (0.8)
Completeness (%)	
Spherical	71.2 (24.9)
Elliptical**	92.8 (91.4)
Redundancy	34.3 (31.7)
Wilson B ($Å^2$)	149.4
Refinement	
Resolution (Å)	48.6 – 3.8
No. reflections	18489
R_{work} / R_{free}	28.1 / 31.7
No. atoms	
Protein	10838
Ligand/ion	NA
Water	NA
B-factors ($Å^2$)	
Protein	193.5
Ligand/ion	NA
Water	NA
R.m.s. deviations	
Bond lengths (Å)	0.01
Bond angles (°)	1.15

*Values in parentheses are for highest-resolution shell.

** Elliptical diffraction limits and principal reciprocal axes of the fitted ellipsoid: 4.6 Å along 0.987 a* - 0.158 c*, 4.4 Å along b* and 3.8 Å along c*

Supplementary Table 2. Intermolecular BamA-RcsF crosslinks detected.

PSMs = Peptide Spectrum Matches. The POTRA domain in BamA where the crosslinked residue is located is also indicated.

BamA Residue	RcsF Residue	BamA Peptide			RcsF Peptide			PSMs	POTRA
		Sequence	Start	End	Sequence	Start	End		
310	61	**K**LLGR	310	314	IYTNAEELVG**K**PFR	51	64	3	4
361	42	FEGND**TSK**DAVLR	354	366	AEPAKP**K**APR	36	45	3	5
361	61	FEGND**TSK**DAVLR	354	366	IYTNAEELVG**K**PFR	51	64	78	5
310	134	**K**LLGR	310	314	QAVCIGSALNITA**K**	121	134	1	4
417	61	VPGSPDQVDVVY**K**VK	405	419	IYTNAEELVG**K**PFR	51	64	14	5
419	61	V**K**ER	418	421	IYTNAEELVG**K**PFR	51	64	24	5

N.B. Residue 134 is the C-terminal Lys of RscF

Supplementary Table 3. Strains used in this study.

Strains	Genotype and description	Source
BL21 (DE3)	F- *ompT hsdSB* (rB- mB-) *gal dcm* (DE3)	Novagen
DH300	*rprA-lacZ* MG1655 *(argF-lac) U169*	[32]
PL339	Δ*rcsF::kan*	[10]
PL358	DH300 Δ*rcsF*	[10]
Keio collection single mutants	Δ*rcsF::kan*	[33]
RRA73	BL21 (DE3) with pRRA1	This study
RRA74	BL21 (DE3) with pRRA1 and pSC216	This study
SEN1071	PL358 with pJH118 and pSC216	This study
SEN1472	DH300 Δ*bamA::kan* with pSC270	This study
SEN1603	DH300 Δ*bamA::kan* with pBamA	This study
SEN1607	DH300 Δ*bamA::kan* with $pBamA_{\Delta loop1}$	This study
SEN1411	DH300 with pET3a and pAM238	This study
SEN991	DH300 with pBamA and pAM238	This study
SEN1597	DH300 with pBamA-B and pAM238	This study
SEN1598	DH300 with pBamA-B and pSC263	This study
RRA54	DH300 with $pBamA^{G393C/G584C}$-B and pAM238	This study
RRA106	DH300 with $pBamA^{G433C/N805C}$-B and pAM238	This study
SEN1723	DH300 Δ*bamA::kan* with $pBamA^{hinge}$	This study

Supplementary Table 4. Plasmids used in this study.

Plasmids	Features	Source
pAM238	IPTG-regulated Plac, pSC101-based, spectinomycin	[57]
pBAD33	Arabinose regulation, pACYC184-based, chloramphenicol	[58]
pSC231	pAM238 with $LacI^q$ and the modified P_{trc}	[10]
pSIM5-tet	pSC101-based, *repA*^{ts}, tetracycline	[35]
pSUPAR-Mb-Dizpk-RS	PylRS, $tRNA^{Pyl}_{CUA\ opt}$, p15A origin, chloramphenicol	[24]
pET3a	T7 promoter, ampicillin	Novagen
pTrc99a	IPTG-regulated P_{trc}, ampicillin	[59]
pBamA	pET23a with BamAss-6xHis-2xAla-BamA(E22-W810), Ampicillin	[10]
pBamA^{hinge}	pBamA (BamA with the insertion of a LVPR sequence at position 424)	This study
pBamA$_{\Delta loop1}$	pBamA (BamA with the deletion from T434-G437)	This study
pBamA-B	pBamA::BamB	This study
pBamA$^{G393C/G584C}$-B	pBamA$_{L6}$-B with BamA$^{G393C/G584C}$	This study
pBamA$^{G433C/N805C}$-B	pBamA$_{L6}$-B with BamA$^{G433C/N805C}$	This study
pSC263	pAM238 with BamCDE, spectomycin	This Study
pSC216	pBAD33 with RcsF	[10]
pJH114	pTrc99a::BamA-BamB-BamC-BamD-BamE-6×His	[36]
pJH118	pTrc99a::6×His-BamA-BamB	[36]
pRRA1	pJH114 but with modifications: 6×His-BamA and BamE with no 6×His	This study
pSC270	pSC231 with BamA	This study
pSC270^{R583X}	amber codon (TAG) replacing the codon for the designated amino acid residues	This study
pSC270^{R592X}	amber codon (TAG) replacing the codon for the designated amino acid residues	This study
pSC270^{R598X}	amber codon (TAG) replacing the codon for the designated amino acid residues	This study
pSC270^{R610X}	amber codon (TAG) replacing the codon for the designated amino acid residues	This study
pSC270^{R632X}	amber codon (TAG) replacing the codon for the designated amino acid residues	This study

pSC270 ^{R634X}	amber codon (TAG) replacing the codon for the designated amino acid residues	This study
pSC270 ^{R661X}	amber codon (TAG) replacing the codon for the designated amino acid residues	This study
pSC270 ^{K808X}	amber codon (TAG) replacing the codon for the designated amino acid residues	This study

Supplementary Table 5. Primers used in this study.

Name	Sequence (5' to 3')
bamB (NotI) R	GAGAGCGGCCGCTTAACGTGTAATAGAG
pTrc-for	CAAGGCGCACTCCCGTTCTGG
pTrc-rev2	CGCCAGGCAAATTCTG
BamA (PciI)F	GAGACATGTTGGCGATGAAAAAGTTGC
BamA (XbaI)R	GAGTCTAGATTACCAGGTTTTACCG
bamC kpnI F	GATCGGTACCTCGGATCTTAGGGAGATTTGATGGC
bamA Km del F	GATTTCTCTCGGTTATGAGAGTTAGTTAGGAAGAACG CATAATAACGATGATTCCGGGGATCCGTCGACC
bamA Km del R	CTACCACTACATTCCTTTGTGGAGAACACTTACCAGG TTTTACCGATGTTTGTAGGCTGGAGCTGCTTCG
SDM-His-BamA F	CACCATCACCACCATGGCGCGGCCGAAGGGTTCGTA GTGAAAGATATTCATTTCG
SDM-His-BamA R	CGCCATGGTGGTGATGGTGATGGGCCGCGTATACGG TGGCG
bamE delHis F	TGCGCTGAGTGGTAACTAAGATCCTCTAGAGTCGAC
bamE delHis R	GTCGACTCTAGAGGATCTTAGTTACCACTCAGCGCA
BamA Hinge F	GTAAAAGAGCGCAACACCCTGGTGCCGCGCGGTAGC TTCAACTTTGGT
BamA Hinge R	ACCAAAGTTGAAGCTACCGCGCGGCACCAGGGTGTT GCGCTCTTTTAC

1040

1041 **Supplementary Video**

1042 **Dynamic importance sampling (DIMS) simulation of the BamA-RcsF complex**
1043 **reproducing the proposed push-and-pull model.** The simulation shows the transition
1044 of BamA from the inward-open to the outward-open conformation, with the POTRA5
1045 domain moving towards the periplasmic exit of the lumen and pushing RcsF upwards.
1046 This movement is accompanied later on by the movement of strands 1-6 in BamA (Z1
1047 domain) and the opening of the outward-facing extremity. The initial conformation of
1048 the system (BamA and RcsF) corresponds to the inward-open structure determined in
1049 this work (PDB code 6T1W) with the POTRA1-4 domains removed. The final
1050 conformation of BamA is similar to the outward-open structure (PDB code 5D0Q). The
1051 proteins are represented as cartoons (BamA and RcsF colored in orange and blue,
1052 respectively), the explicit outer membrane represented as sticks and the oxygen atoms
1053 of water molecules represented as red dots.

1054